Energy cascade in multi-mode stretched spiral vortex and viscoelastic effect

Kiyosi Horiuti (Tokyo Institute of Technology, Japan)

Collaborators: Y. Takagi, T. Fujisawa, M. Koike, K. Saitou, K. Kawamura, K. Matsumoto

Temporal development of coherent structures in isotropic turbulence box

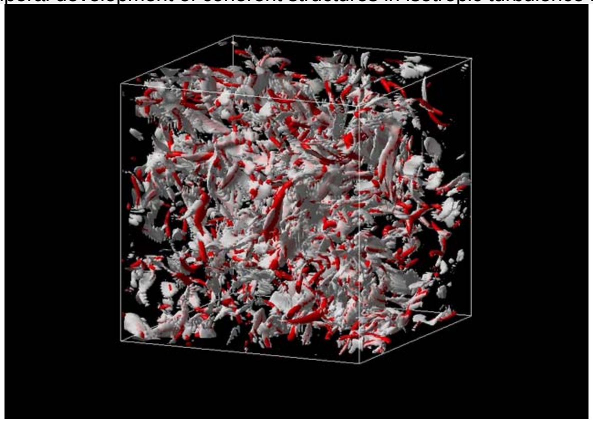

Red isosurfaces: tubular object; White isosurfaces: planar object

Motivation

- Existence of organized vortical structures, termed ribbons, blobs, and worms has been known (e.g., Jimenez & Wray 1998).
- The primary elements of vortical structures are the tube-like object and the sheet (or layer)-like object. These objects are not separable since local dissipation is particularly strong, not within vortex tubes, but rather in their neighbourhood (e.g. Kerr 1985).
- A model of generalized Burgers vortices for the small-scale structure of turbulence was introduced in Lundgren (1982). In this model (LSV), vortex sheets are stretched in the spiral to continually tighten, and this mechanism causes an energy cascade. The LSV model gives the $k^{-5/3}$ energy spectrum.

Objective

- Extract LSVs and analyse their complete creation process in homogeneous isotropic turbulence.
- Explore the roles of the LSVs on generation of turbulence energy cascade and dissipation.
- Explore a possibility of achieving turbulence control through the suppression of formation of LSV (in polymer-diluted flow).

Motivation

• Existence of organized vortical structures, termed ribbons, blobs, and worms has been known (e.g., Jimenez & Wray 1998).
• The primary elements of vortical structures are the tube-like object and the sheet (or layer)-like object. Local dissipation is particularly strong, not within vortex tubes, but rather in their neighbourhood (e.g. Kerr 1985).
• A model of generalized Burgers vortices for the small-scale structure of turbulence was introduced in Lundgren (1982). In this model (LSV), vortex sheets are stretched in the spiral to continually tighten, and this mechanism causes an energy cascade. The LSV model gives the Kolmogorov $k^{-5/3}$ energy spectrum

Objective

• Extract LSVs and analyse their complete creation process in homogeneous isotropic turbulence.
• Explore the roles of the LSVs on generation of turbulence energy cascade and dissipation.
• Explore a possibility of achieving turbulence control through the suppression of formation of LSV (in polymer-diluted flow).

Identification method for turbulent structures (1)

Tubular structure in biaxial elongational flow

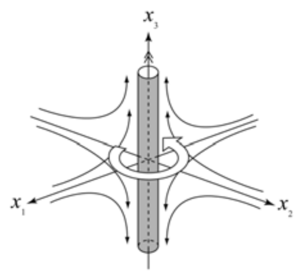

Sheet structure in planar elongational flow

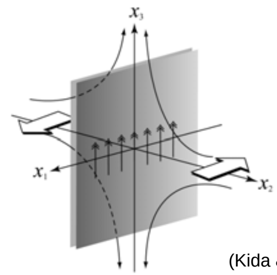

(Kida & Yanase)

Vortex tube: $\Omega_{ik}\Omega_{ik} >> S_{ik}S_{ki}$
- Pressure, p.
- 2nd-order invariant of the velocity gradient tensor, Q

Vortex sheet: $\Omega_{ik}\Omega_{ik} \sim S_{ik}S_{ki}$

Eigenvalue of the 2nd-order tensor of the velocity gradient tensor,

$[A_{ij}]_+$, $[A_{ij}] \equiv S_{ik}\Omega_{kj}+S_{jk}\Omega_{ki}$ (Horiuti & Takagi 2005, PoF)

Identification method for turbulent structures (3)

Performance of identification method

Comparison with other fourth order velocity gradient invarients

Burgers' vortex layer

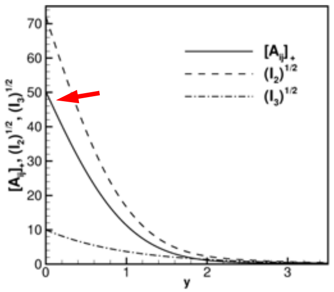

Burgers' vortex tube

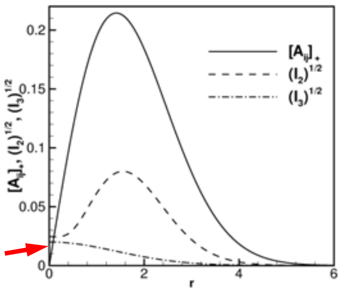

Contours of $[A_{ij}]_+$ on Q

Newtonian

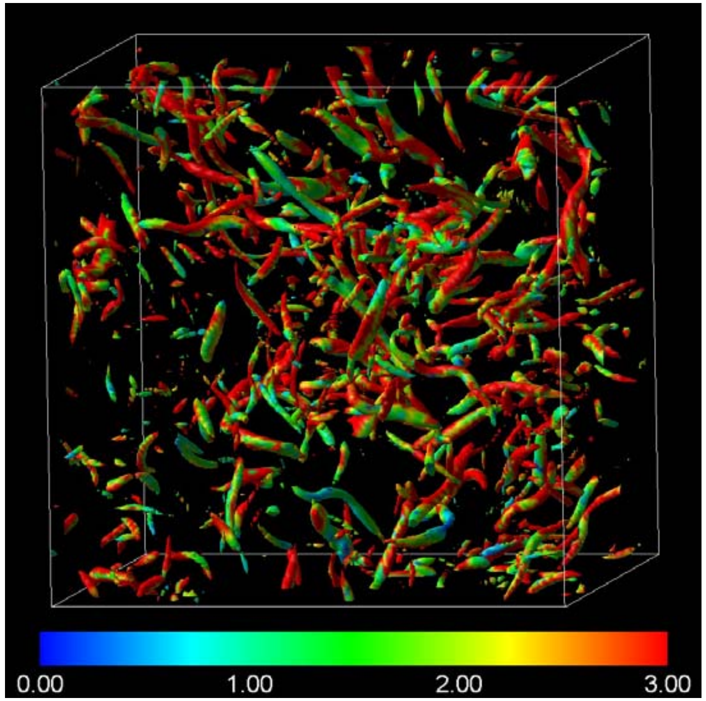

Identification method for turbulent structures (2)

Reordering of eigenvalues

Based on degree of alignment of their eigenvectors with vorticity vector ω

z or s Maximumly aligned with, ω: σ_z, $\boldsymbol{e}_z$ (z or s)

Largest among remainder: σ_+, $\boldsymbol{e}_+$

Smallest eigenvalue: σ_-, $\boldsymbol{e}_-$

(Andreotti 1993)

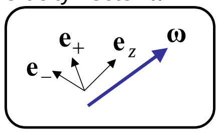

Vectors and tensors on the basis of strain rate eigenvectors

- Vector, Vortex stretching term

$$\omega_z = \boldsymbol{\omega}\cdot\boldsymbol{e}_z,\ \omega_+ = \boldsymbol{\omega}\cdot\boldsymbol{e}_+,\ \omega_- = \boldsymbol{\omega}\cdot\boldsymbol{e}_-$$

- Tensors: ex) Pressure Hessian term

$$\tilde{\Pi}_{ij} = \mathrm{E}^{\mathrm{T}}(\Pi_{ij})\mathrm{E},\quad \Pi_{ij} = \frac{\partial^2 p}{\partial x_i \partial x_j},\quad \mathrm{E} = (e_+, e_-, e_z)$$

Alternatively, eigenvalues and eigenvectors of $[A_{ij}]$ are used:

$$[A_{ij}]_z,\ [A_{ij}]_+,\ [A_j]_-,\ \boldsymbol{a}_z,\ \boldsymbol{a}_+,\ \boldsymbol{a}_-$$

Crossover of strain-rate tensor eigenvalues

Conventional ordering of eigenvalues: $\sigma_1 > \sigma_2 > \sigma_3$

Burgers' vortex tube

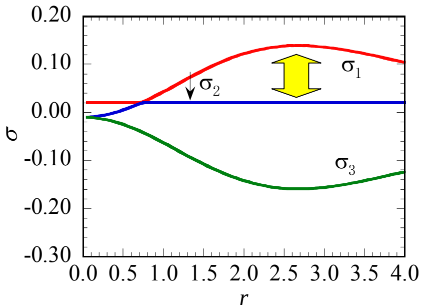

Burgers' vortex layer

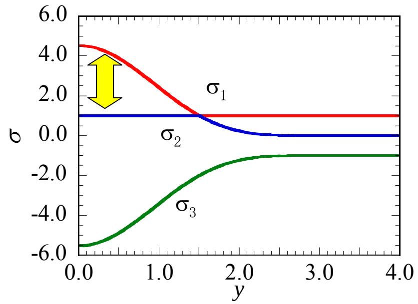

Alignment of the eigenvector for the second largest eigenvalue with the vorticity vector (Kerr *et al.* 1985).

Profiles of homogeneous-isotropic DNS data

Grid-point #		R_λ	$k_{max}\eta$	$\langle K \rangle$	$\langle \varepsilon \rangle$	L	λ	η x 10^{-3}
256^3	Decay	77.2	1.02	0.90	0.65	0.47	0.14	8.00
512^3	Decay (Low Re)	76.9	2.05	0.90	0.65	0.47	0.14	8.00
1024^3	Decay (Low Re)	77.4	4.09	0.90	0.65	0.47	0.14	8.00
1024^3	Decay (High Re)	122.5	1.35	0.96	0.30	0.47	0.09	2.63
512^3	Forced (1.0<k<2.5)	158.1	2.27	1.41	0.40	1.26	0.22	8.91
1024^3	Forced (1.0<k<2.5)	243.3	2.49	1.43	0.39	1.14	0.15	4.89

Assessment using the DNS data

- Homogeneous isotropic turbulence (decaying)

  Initial energy spectrum:

$$E(k) = C\,k_p^{-1}\left(\frac{k}{k_p}\right)^8 \exp\left\{-2\left(\frac{k}{k_p}\right)^2\right\}, \quad k_p = 2$$

- Homogeneous shear turbulence

Advantage of use of eigenvalue, $[A_{ij}]_+$

- Vortex sheet is approximately spanned by the eigenvectors for $[A_{ij}]_z$ and $[A_{ij}]_-$, noting that $grad([A_{ij}]_+)$ is nearly perpendicular to the surface of the sheet.

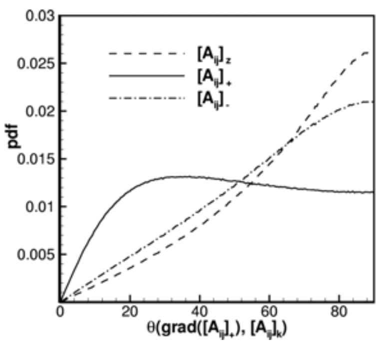

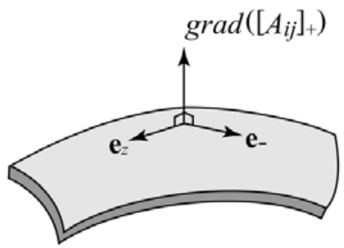

Formation of vortex tube via conventional rolling-up of a (single) vortex sheet

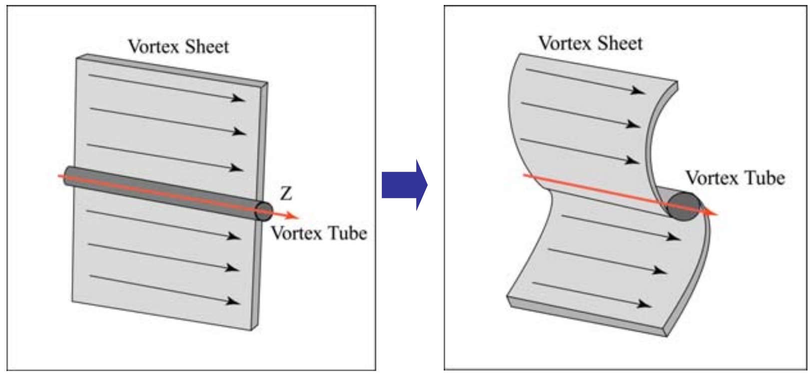

The vortex tube is formed through focusing of vorticity along a single vortex sheet (Neu 1984, Kerr & Dold 1994).

Formation of vortex tube via conventional rolling-up

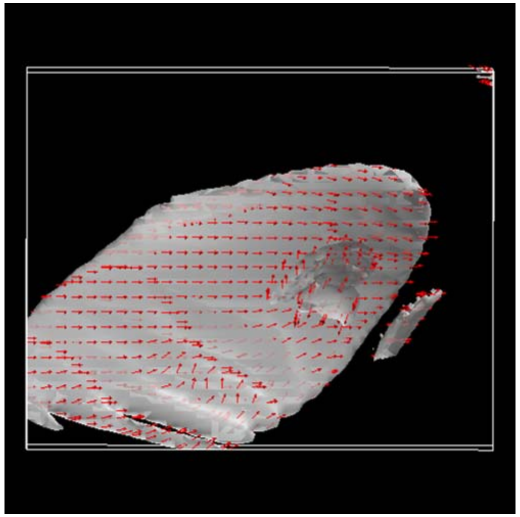

White isosurface:
vortex sheet

Red isosurface:
vortex tube

Red vectors:
vorticity vector

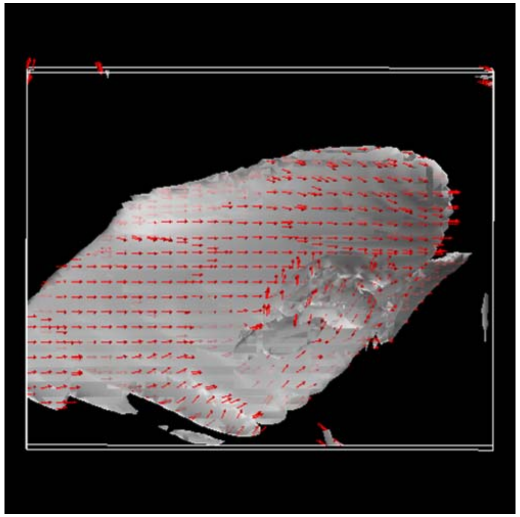

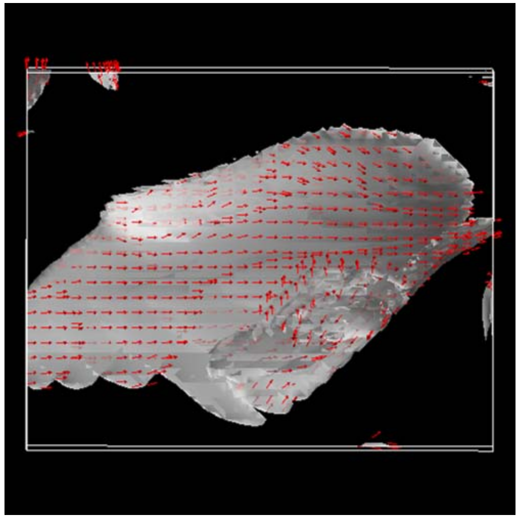

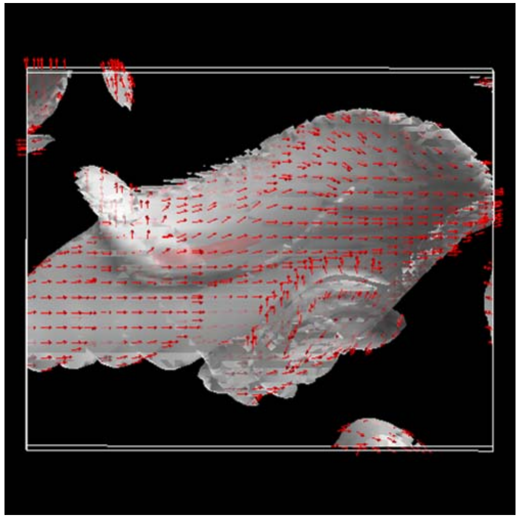

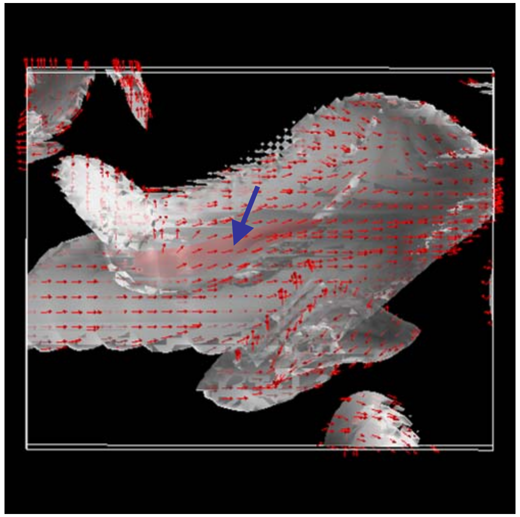

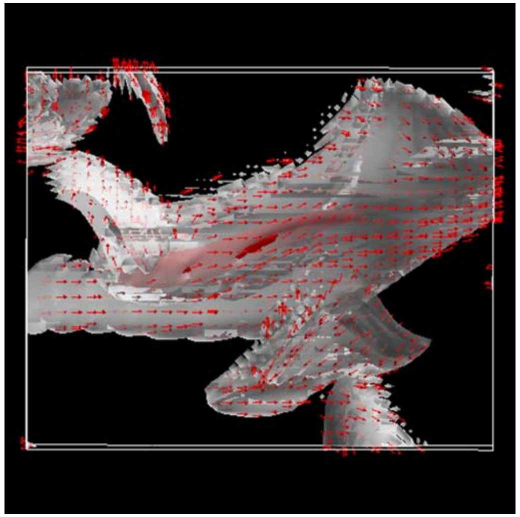

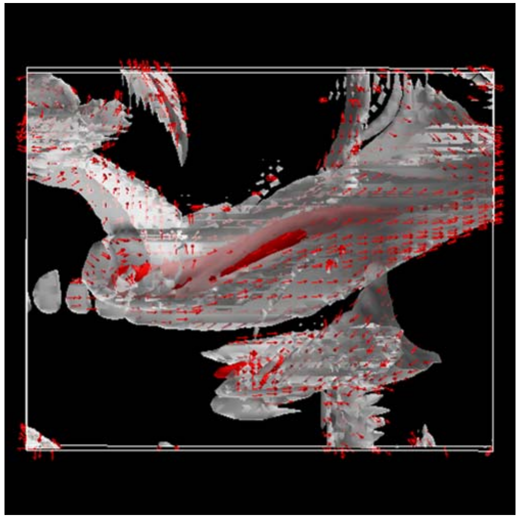

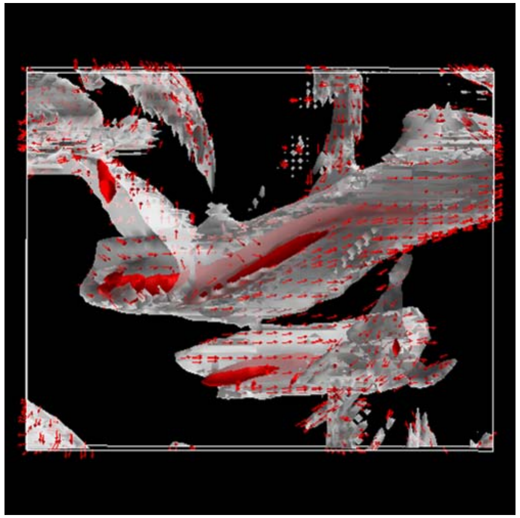

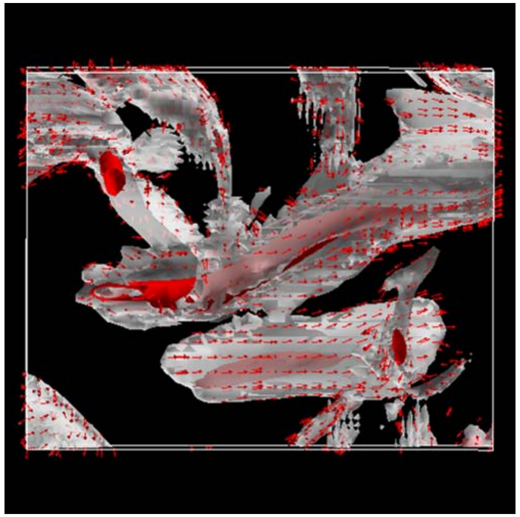

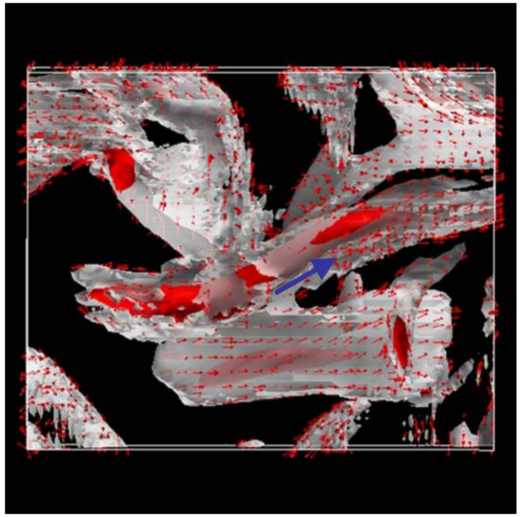

Vorticity vectors are always aligned with the longitudinal direction of the tube.

Origin of the tube in the development of the rolled-up vortex sheet

Rolled-up sheet | Initial condition

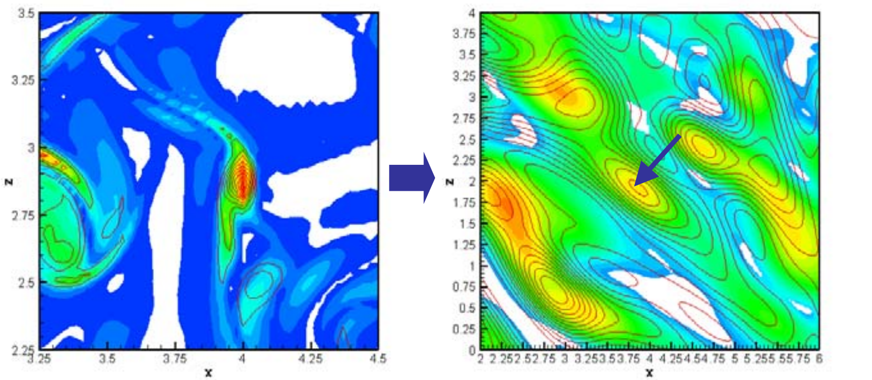

Traced back to the concentration of vorticity along the sheet
in the initial velocity field.
The vortex tube is formed through focusing process (Neu 1984).

Multi-mode stretched spiral vortex

3-dimensional rendering

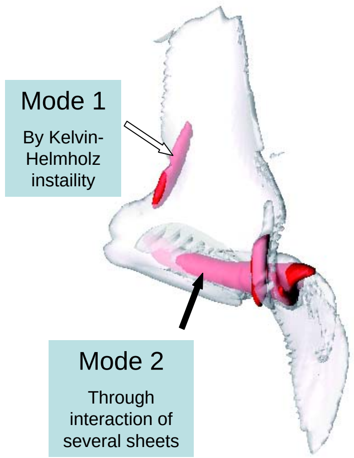

Topological classification with regards to vorticity alignment along the two sheets and the tube

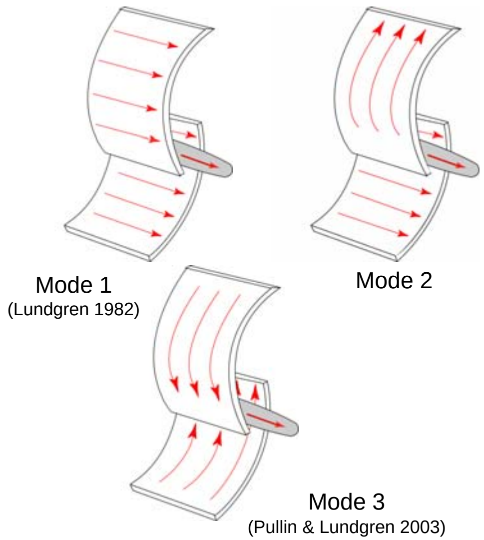

A process of formation of stretched spiral vortex

Configuration in early stage

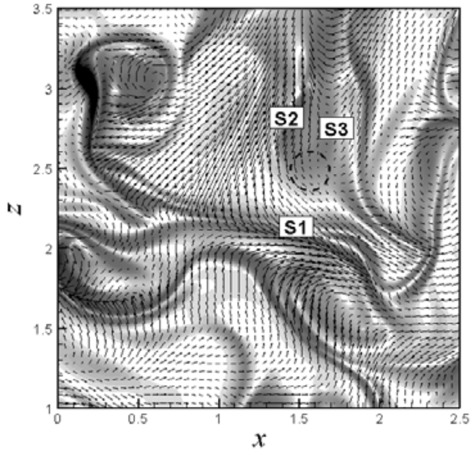

- Consists of a lot of stagnation flows caused by vortex sheets.
  (Davila and Vassilicos 2003)
- Straining and stretching of the vortex blob along the sheets.
  (Gilbert 1993)

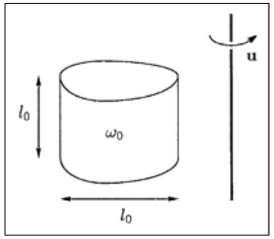

- Mostly in Mode 3, converted into Mode 1 or Mode 2 with lapse of time.

A process of formation of stretched spiral vortex

Initial configuration

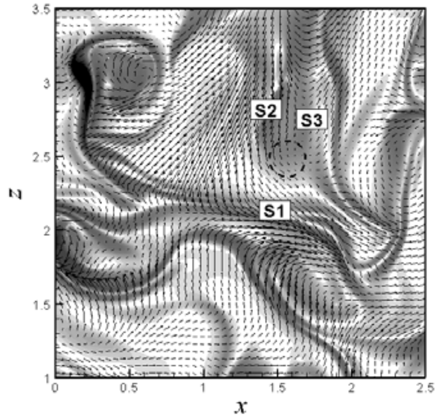

Mostly in Mode 3

Summary of the process

- Appearance of the stagnation flow.
- Generation of recirculating flow.
- Straining and stretching of the sheets by the recirculating flow.
- Reorientation the vorticity directions along the stretched sheets due to the action of the pressure Hessian term.
- Creation of the vortex tube by concentration of the recirculating flow.

A process of formation of stretched spiral vortex

Initial configuration

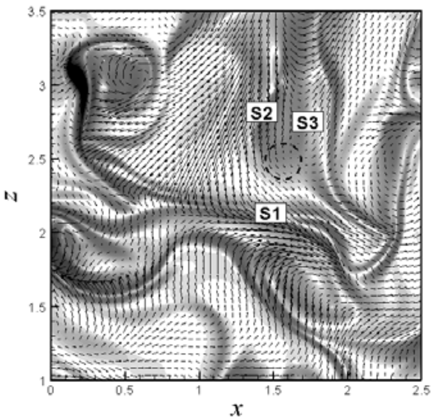

Mostly in Mode 3

Summary of the process

- Appearance of the stagnation flow along the vortex sheets.
- Generation of recirculating flow through interaction with another sheet.
- Straining and stretching of the sheets by the recirculating flow.
- Reorientation the vorticity directions along the stretched sheets due to the action of the pressure Hessian term.
- Creation of the vortex tube by axial straining and concentration of the low pressure region in the recirculating flow.

A process of formation of stretched spiral vortex

Distribution of sheets at an early stage

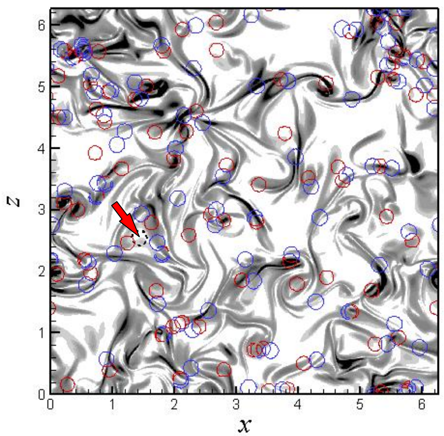

○ : swirling flow, ○ : stagnation flow

Index number

Summary of the process

- Different from rolling up of the layer due to Kelvin-Helmholz instability.
- Created through the interaction of several sheets.
- Convergence of recirculating flow and concentration of its low-pressure region.

(Waleffe 2003)

A process of formation of stretched spiral vortex

Contours of vortex sheets and pressure

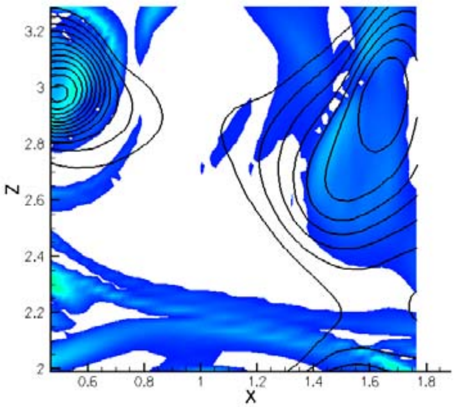

- Different from rolling up of the layer due to Kelvin-Helmholz instability.
- Created through the interaction of several sheets.
- Similar to the process considered for wall turbulence by Waleffe (2003).

A process of formation of stretched spiral vortex

Gray scale : vortex sheet, Vectors: velocity

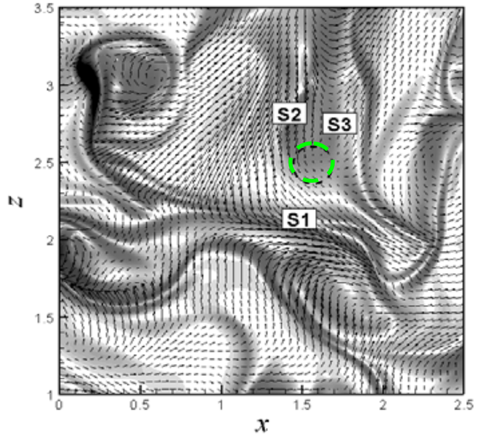

$t = 1.05$

- Initial configuration consists of by a stagnation flows caused by vortex sheets.(Davila and Vassilicos 2003)
- The following process is composed of by the three phases.

1. Genesis phase
2. Growth phase
3. Annihilation phase

Genesis phase of LSV

Generation of recirculating flow by convergence of the stagnation flow.

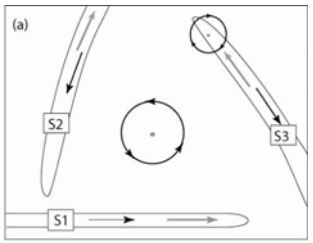

Interaction with the vortex on the third sheets.

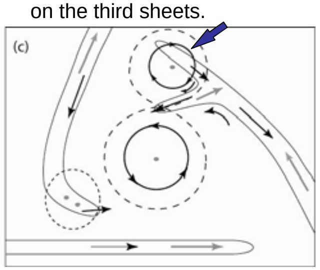

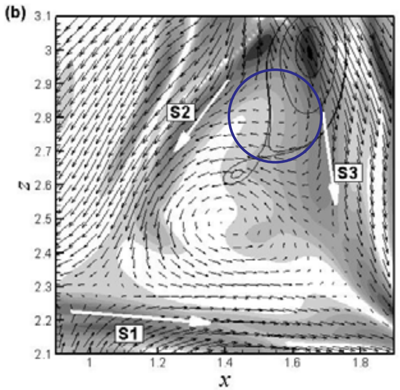

In Mode 3

Straining and stretching of vortex sheets by recirculating flow and the swirling flow caused by the vortex along S3.

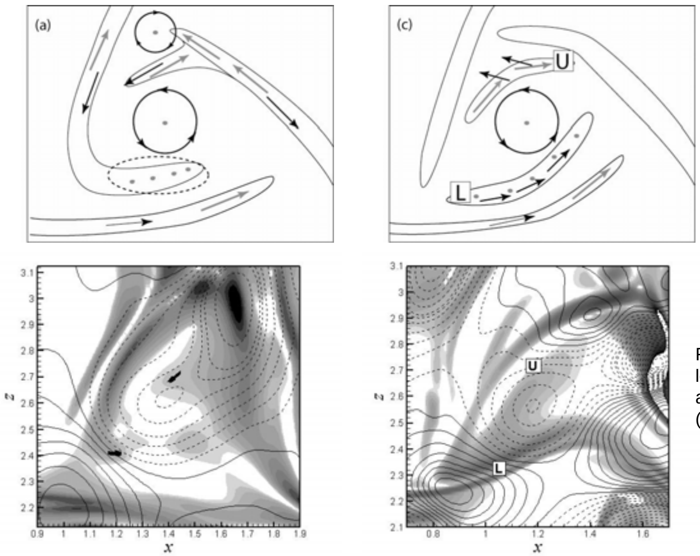

Formation of lower (L) and upper (U) sheets

Creation of the vortex tube in the core region of LSV

- Absorption of the low pressure region in the recirculating flow into the lower sheet L.
- Stretching due to axially straining fields induced by the vortices in near neighbors.
- Concentration of the vorticity in the low pressure region.

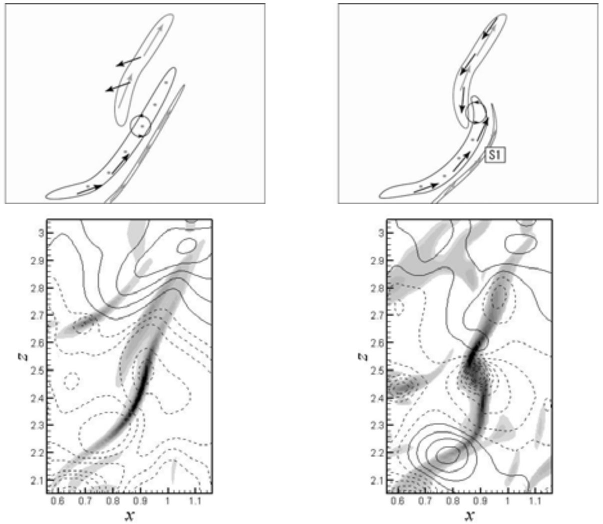

Creation of vortex tube by axial straining and concentration of low pressure region.

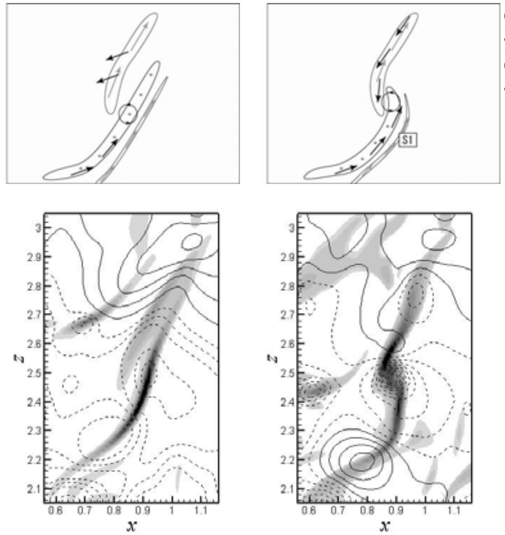

- Entrainment of vortex sheets by the tube, causing the sheets to form a spiral.
- Lowering of pressure and intensification of swirling motion.
- This spiral tightens and form spiral turns.

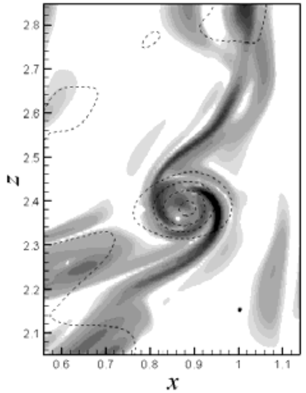

Fractal properties of spiral
(Vassilicos & Brasseur 1996)

Growth phase of LSV

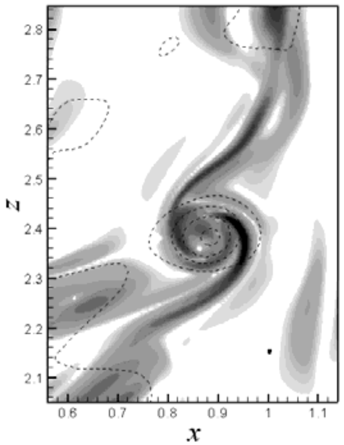

- Decrease of the area of the cross section of the tube
- Concentration of the vorticity
- Further stretching of lower and upper sheets
- Entrainment of vortex sheets by the tube, causing the sheets to form a spiral
- This spiral tightens and form spiral turns

Generation of intense dissipation along the spiral arms

Schematic sketch of streamwise vortex formation process in sheared turbulence

(Waleffe 2003)

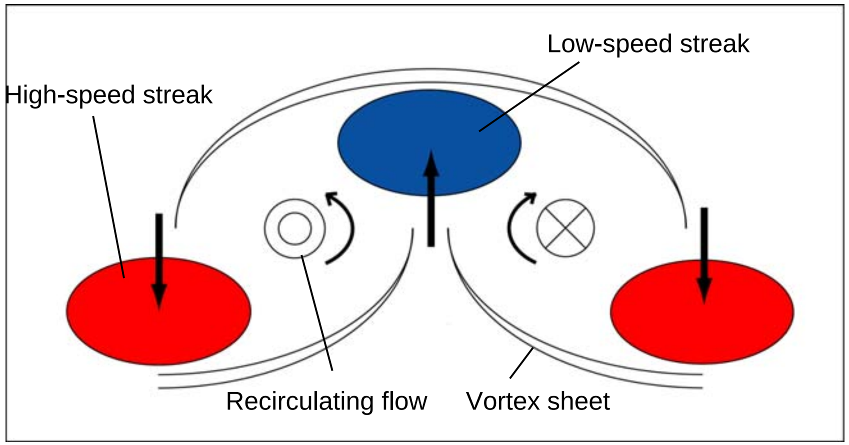

Inter-mode transition in stretched spiral vortex

Initial configuration: Mode 3
⇒ Occurrence of reorientation of vorticity vector

Vortex stretching term: $\sigma_z \omega_z^{\,2}$

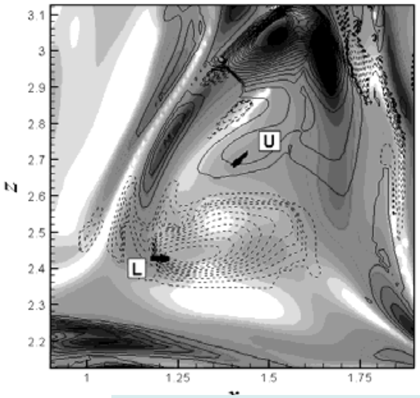

Converted to Mode 2

$\tilde{\Pi}_{zz}$

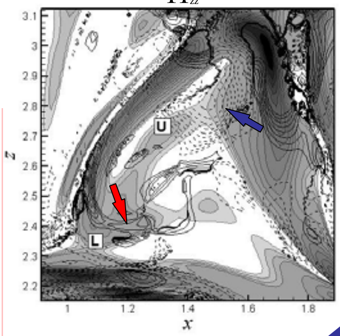

$$\frac{D}{Dt}\sigma_z = -\sigma_z^2 + \left(\omega_+^2 + \omega_-^2\right)/4 - \Pi_{zz}$$

On upper sheet U :

$$\tilde{\Pi}_{zz} < 0 \Rightarrow \sigma_z \nearrow \Rightarrow \sigma_z > 0$$

On lower sheet L :

$$\tilde{\Pi}_{zz} > 0 \Rightarrow \sigma_z \searrow \Rightarrow \sigma_z < 0$$

Mechanism for occurrence of reorientation of vorticity direction

Governing equation for σ_z
on the $\boldsymbol{e}_z$, $\boldsymbol{e}_+$, $\boldsymbol{e}_-$ basis

$$\frac{D}{Dt}\sigma_z = -\sigma_z^2 + \frac{1}{4}\left(\omega_+^2 + \omega_-^2\right) - \tilde{\Pi}_{zz}$$
$$\frac{D}{Dt}\sigma_+ = -\sigma_+^2 + \frac{1}{4}\left(\omega_z^2 + \omega_-^2\right) - \tilde{\Pi}_{++}$$

Horiuti & Fujisawa (2008)

$\tilde{\Pi}_{zz}$

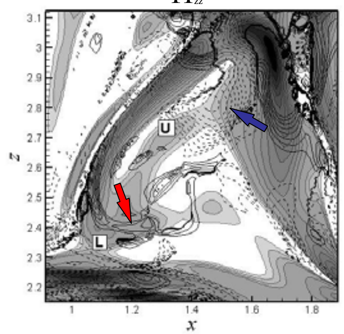

On upper sheet U :

$$\tilde{\Pi}_{zz} < 0 \Rightarrow \frac{D}{Dt}\sigma_z > 0 \Rightarrow \sigma_z \nearrow \Rightarrow \sigma_z > 0$$

On lower sheet L :

$$\tilde{\Pi}_{zz} > 0 \Rightarrow \frac{D}{Dt}\sigma_z < 0 \Rightarrow \sigma_z \searrow \Rightarrow \sigma_z < 0$$

Inter-mode transition of stretched spiral vortex

Example of Mode 3 – Mode 1 transition

Distribution of sheets and velocity

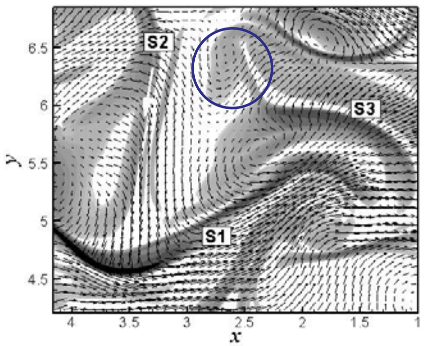

Formation of recirculating flow
by an interaction of three sheets

$\tilde{\Pi}_{zz}$

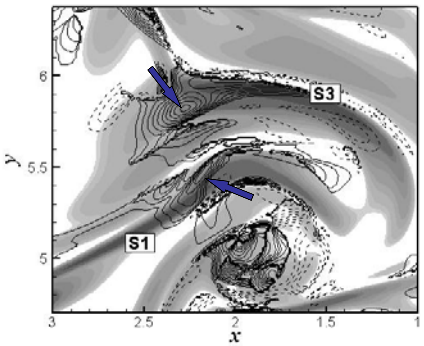

$\tilde{\Pi}_{ss}$ > 0 on both sheets
→ Occurrence of reorientation on both sheets

Appearance for Mode 3-2 and 3-1 transitions

Mode 3 – 2 transition

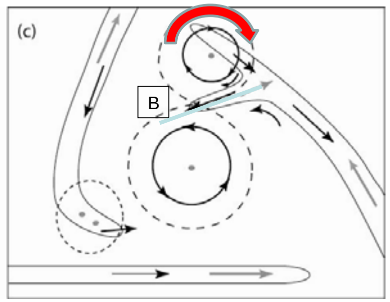

Pressure distribution is <u>convex</u> near the branching point (B) of pressure.

$\tilde{\Pi}_{zz}$ < 0 on upper sheet
$\tilde{\Pi}_{zz}$ > 0 on lower sheet
→ Occurrence of reorientation only on lower sheet

Mode 3 – 1 transition

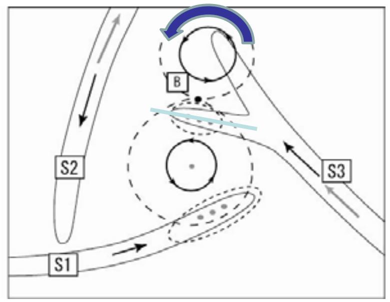

Pressure distribution is <u>concave</u> on both sheets.

$\tilde{\Pi}_{zz}$ > 0 on both sheets

➔ Occurrence of reorientation on both sheets

Inter-mode transition in stretched spiral vortex

Initial configuration: Mode 3
⇒ Occurrence of reorientation of vorticity vector direction

Vortex stretching term: $\sigma_z \, \omega_z^{\,2}$

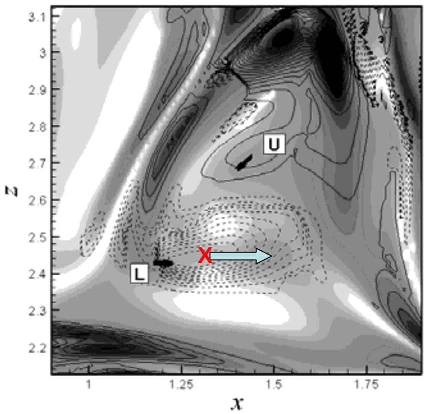

Velocity direction on S3

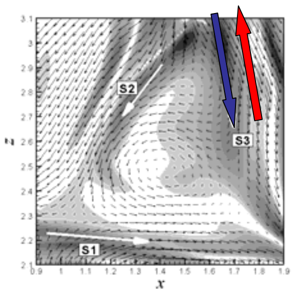

The same as those on S1 and S2:
Mode 3 ⇒ Mode 1

Opposite to those on S1 and S2:
No reorientation takes place

$$\frac{D}{Dt}\sigma_z = -\sigma_z^2 + \frac{1}{4}\left(\omega_+^2 + \omega_-^2\right) - \tilde{\Pi}_{zz}$$

Occurrence of reorientation of vorticity vector direction

Governing equation for σ_z

$$\frac{D}{Dt}\sigma_z = -\sigma_z^2 + \frac{1}{4}\left(\omega_+^2 + \omega_-^2\right) - \Pi_{zz}$$
$$\frac{D}{Dt}\sigma_+ = -\sigma_+^2 + \frac{1}{4}\left(\omega_z^2 + \omega_-^2\right) - \Pi_{++}$$

Velocity direction on S3

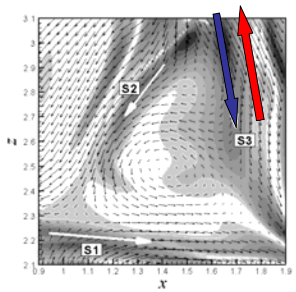

The same as those on S1 and S2:

$$\tilde{\Pi}_{zz} > 0 \;\Rightarrow\; \frac{D}{Dt}\sigma_z < 0 \;\Rightarrow\; \sigma_z \searrow \;\Rightarrow\; \sigma_z < 0$$

Opposite to those on S1 and S2:

$$\tilde{\Pi}_{zz} < 0 \;\Rightarrow\; \frac{D}{Dt}\sigma_z > 0 \;\Rightarrow\; \sigma_z \nearrow \;\Rightarrow\; \sigma_z > 0$$

Mechanism for stretching of the vortex sheet and formation of spiral turns

Differential rotation induced by the tube and that self-induced by the sheet
⇒ stretching, thinning and spiralling of vortex sheets to extreme length.

(Lundgren 1982)

A measure for the strength of the differential rotation

$$D = r\frac{\partial}{\partial r}\left(\frac{u_\theta}{r}\right)$$

Distribution of the *D* term

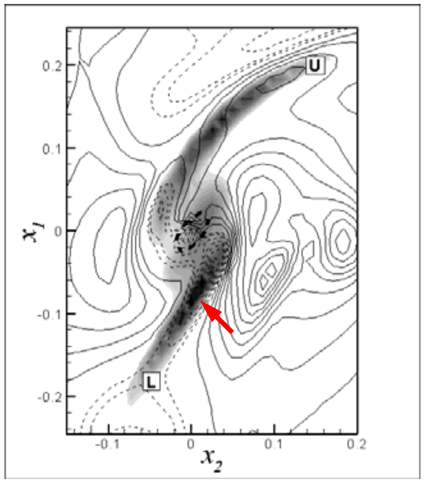

Persistence of three modes

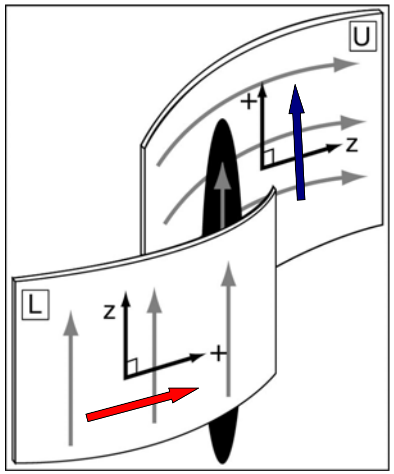

Schematic of configuration on lower and upper sheets in Mode 2

Intense azimuthal velocity is induced by the vortex sheet on the lower sheet L.

Differential rotation induced on the two sheets:
Lower sheet >> Upper sheet

Persistence of Mode 1 configuration

Estimate of average thickness of the vortex sheet, δ

Decrement $\delta(t)$ obtained by fitting the energy spectra with the functional form as $E(k, t) = c(t)\, k^{n(t)}\, e^{-2\delta(t)k}$

(Passot et al. 1995)

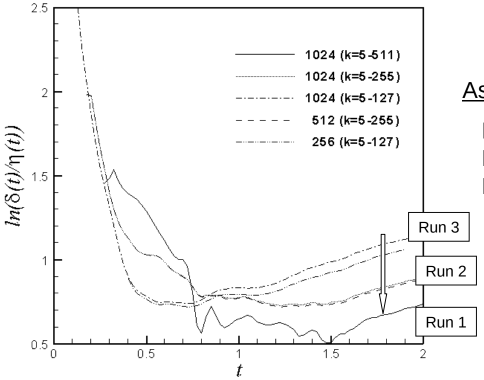

Asymptotic values

Run 1 ($k_{max}\overline{\eta}$ =4.0): 2.05 $\overline{\eta}$
Run 2 ($k_{max}\overline{\eta}$ =2.0): 2.34 $\overline{\eta}$
Run 3 ($k_{max}\overline{\eta}$ =1.0): 3.21 $\overline{\eta}$

No apparent tendency for convergence of the average thickness observed.

Process of formation of stretched spiral vortex (3)

Appearance of spiral turns — Dissipation rate, $\varepsilon/\langle\varepsilon\rangle$

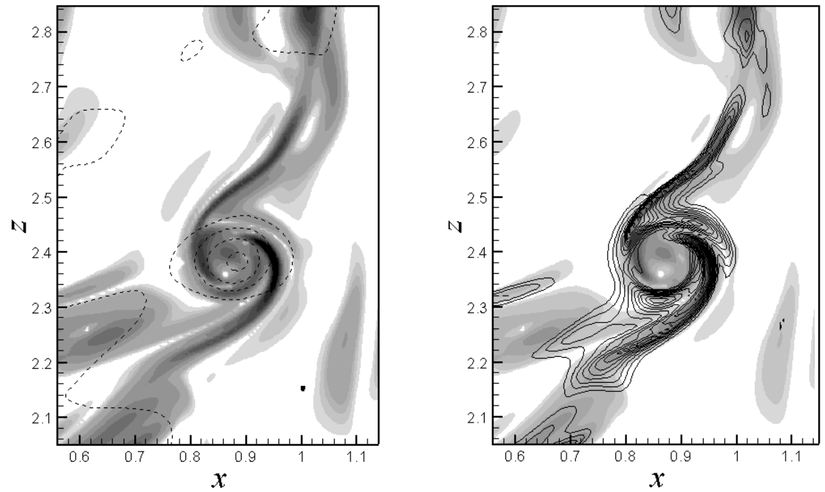

Generation of intense dissipation along the stretched spiral sheets

Process of formation of stretched spiral vortex (3)

Cascade term ($-S_{ik}S_{kj}S_{ji}+\Omega_{ik}\Omega_{kj}S_{ji}$) — Dissipation rate, $\varepsilon/\langle\varepsilon\rangle$

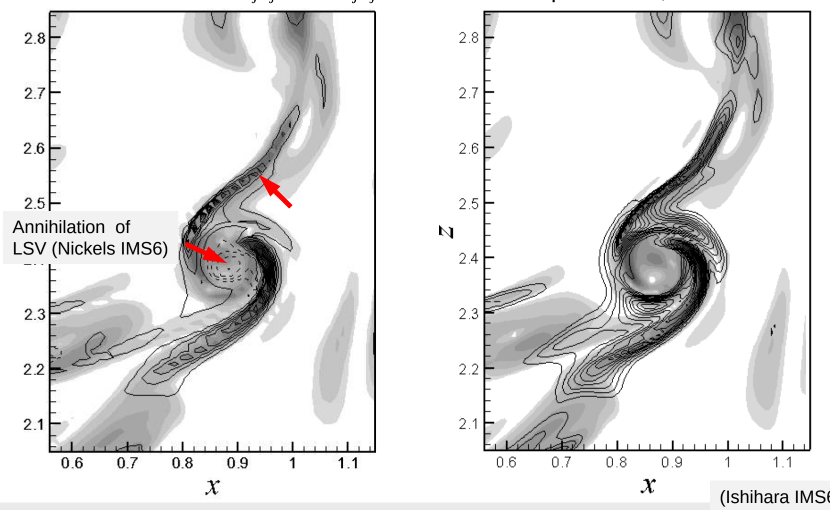

(Ishihara IMS6)

Generation of intense cascade and dissipation along the stretched spiral sheets

Interaction of strain and vorticity

$$\frac{D}{Dt}\left(\frac{1}{2}S_{ij}S_{ji}\right) = -S_{ik}S_{kj}S_{ji} - \omega_i\omega_k S_{ik} - S_{ij}\frac{\partial^2 p}{\partial x_i \partial x_j} + \nu S_{ij}\frac{\partial^2 S_{ij}}{\partial x_k \partial x_k}$$

$$\Updownarrow$$

$$\frac{D}{Dt}\left(\frac{1}{2}\omega_i\omega_i\right) = 2\omega_i\omega_k S_{ik} \qquad -2\nu\Omega_{ij}\frac{\partial^2 \Omega_{ij}}{\partial x_k \partial x_k}$$

Enhancement of vorticity implies reduction of strain (Tsinober et al.(1997))

Strain production term > Vortex-stretching term

Existence of a region with large (concentrated) vorticity:
indispensable for transformation of flat sheet region into vorticity-dominant region

Dissipation and vortex-stretching terms

Dissipation rate $\varepsilon / \langle \varepsilon \rangle$

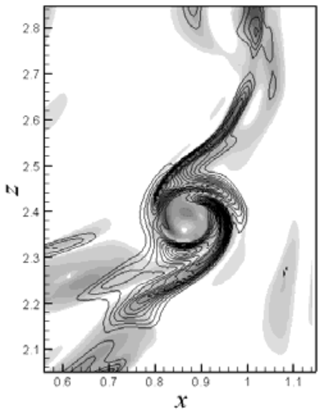

Vortex-stretching term

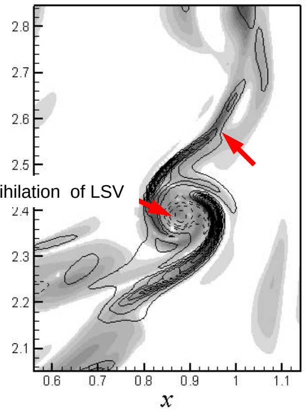

Annihilation phase

The term representing the energy cascade

- Governing equations of the strain rate and enstrophy

$$\frac{D}{Dt}\left(\frac{1}{2}S_{ij}S_{ji}\right) = -S_{ik}S_{kj}S_{ji} - \Omega_{ik}\Omega_{kj}S_{ji} - S_{ij}\frac{\partial^2 p}{\partial x_i \partial x_j} + \nu S_{ij}\frac{\partial^2 S_{ij}}{\partial x_k \partial x_k}$$

$$\frac{1}{2}\frac{D}{Dt}\left(\frac{1}{2}\omega_i\omega_i\right) = 2\Omega_{ik}\Omega_{kj}S_{ji} - 2\nu\frac{\partial^2 \Omega_{ij}}{\partial x_k \partial x_k}$$

- Strain production term + enstrophy production term

  $-S_{ik}S_{kj}S_{ji}+\Omega_{ik}\Omega_{kj}S_{ji}$

  Cf. Estimate obtained using the nonlinear SGS model in LES

⇨ Estimate of the magnitude of energy cascade into small scale

Intense vortex-stretching along the vortex sheets

Superposition of $\Omega_{ik}\,\Omega_{kj}\,S_{ji}$ term and vortex sheets

PIV measurements
O. R. H. Buxton & B. Ganapathisubramani (2010) JFM

$\Omega_{ik}\,\Omega_{kj}\,S_{ji}$ term

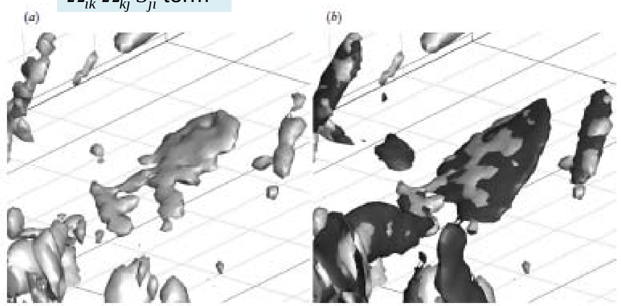

FIGURE 10. (a) An individual example of a sheet of $\omega_i S_{ij} \omega_j$. (b) The same sheet of enstrophy production rate from (a) shown with isosurfaces of $[A_{ij}]_+ = 1.43(\nu/\eta^2)^2$.

Correlation between vortex sheet and vortex-stretching term

$-S_{ik}S_{kj}S_{ji}+\Omega_{ik}\Omega_{kj}S_{ji}$ term on the vortex sheet

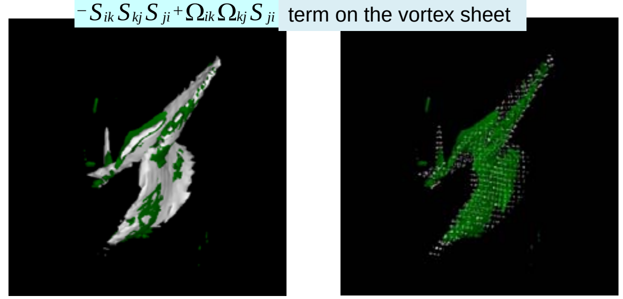

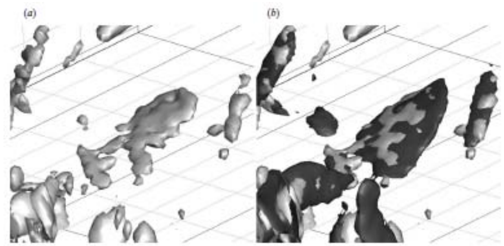

FIGURE 10. (a) An individual example of a sheet of $\omega_i S_{ij} \omega_j$. (b) The same sheet of enstrophy production rate from (a) shown with isosurfaces of $[A_{ij}]_+ = 1.43(\nu/\eta^2)^2$.

$\Omega_{ik}\Omega_{kj}S_{ji}$ term

PIV measurements
O. R. H. Buxton &
B. Ganapathisubramani (2010) JFM

Distributions for indicator for the (small scale) turbulence generation.

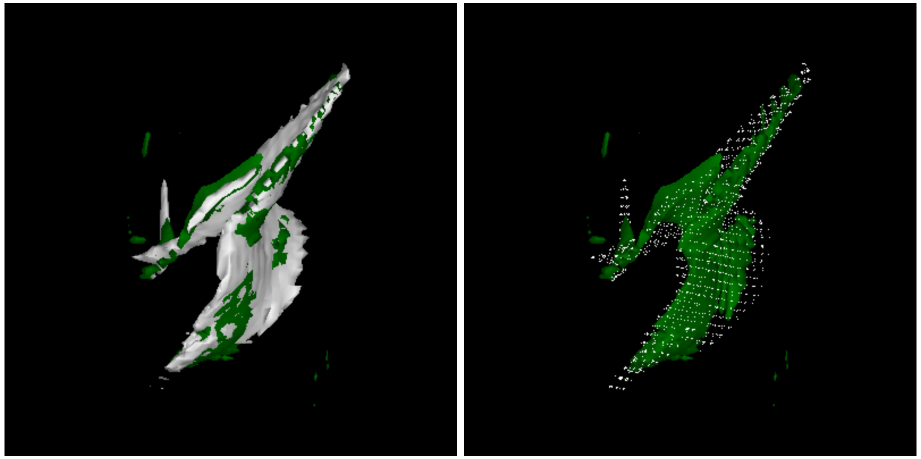

Production term for strain and vorticity: $-S_{ik}S_{kj}S_{ji}+\Omega_{ik}\Omega_{kj}S_{ji}$

Energy cascade in multi-mode stretched spiral vortex

Kiyosi Horiuti (Tokyo Institute of Technology, Japan)

Y. Takagi, T. Fujisawa, K. Saitou, K. Kawamura, K. Matsumoto

PDF of dissipation rate from three Runs.

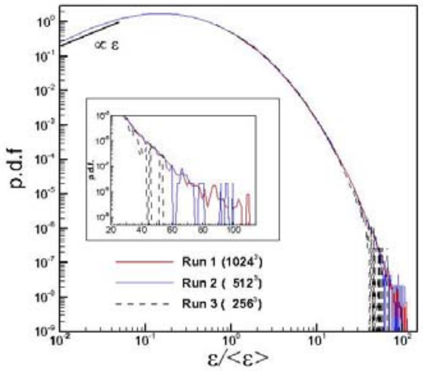

Dissipation field in decaying homogeneous isotropic turbulence

$Re_\lambda \sim 87.0$

Grid resolution:

Run 1 $k_{max}\,\overline{\eta}$ =4.0 (1024^3)

Run 2 $k_{max}\,\overline{\eta}$ =2.0 (512^3)

Run 3 $k_{max}\,\overline{\eta}$ =1.0 (256^3)

$\overline{\eta}$: Averaged Kolmogorov scale

Objective

- Identify the vortical structure responsible for causing turbulent energy dissipation.
- Reveal the formation process for the identified structure.
- Examine the grid resolution requirement for the structures.

Mechanism for stretching of the vortex sheet and formation of spiral turns

Differential rotation induced by the tube and that self-induced by the sheet
⇒ stretching and spiralling of vortex sheets (Lundgren 1982)

A measure for the strength of the differential rotation

$$D = r\frac{\partial}{\partial r}\left(\frac{u_\theta}{r}\right)$$

Stretching and thinning of the spiral sheet to extreme length.
⇒ intense turbulent energy cascade and dissipation

Note: Differential rotation induced on the sheets in Mode 2:
Lower sheet >> Upper sheet
Persistence of Mode 1 configuration

Distribution of the *D* term

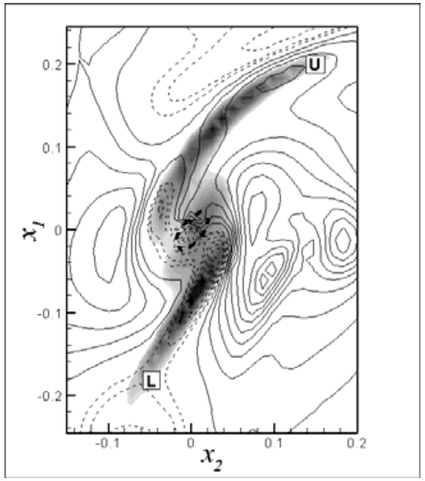

Model for turbulence energy cascade

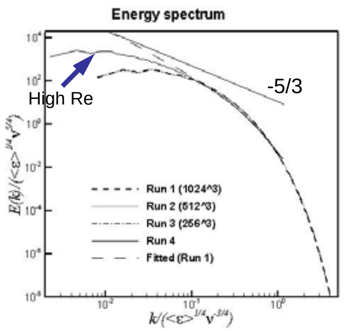

Instability cascade along spiral sheets

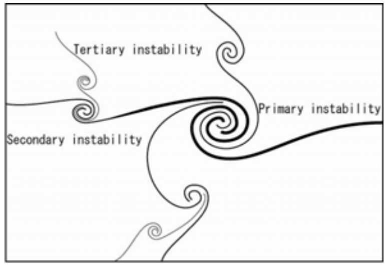

1st generation: LSV with intense vorticity
Confinement of large circulation in the recirculating flow into small cross section
2nd generation: LSV carrying smaller vorticity
Stretching of the spiral arms by 1st generation LSV → Instability of the spiral sheets
3rd generation:
Straining and stretching of the vorticity blobs → Tertiary instability → Rolling up of sheets
………
Formation of hierarchical cluster of self-similar LSV networks
Intermittent cascade of energy to small scales

Scenario for turbulence energy cascade

At higher Reynolds number

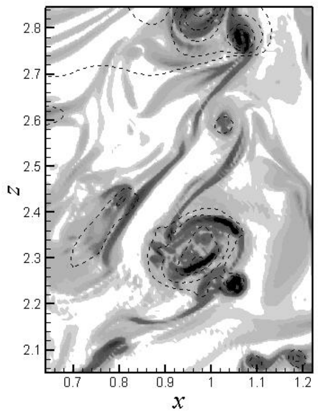

- Formation of hierarchical cluster of self-similar LSV networks
- Cascade of energy to small scales

Instability cascade along spiral sheets

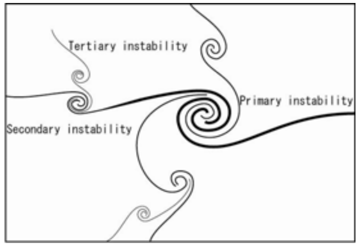

Richardson's scenario for cascade

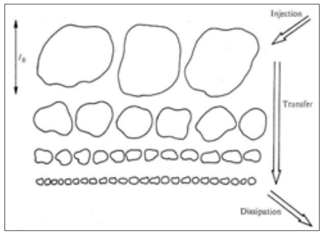

Frish et al. (1978)

LSV formation at a higher Reynolds number

Higher Reynolds numbers:

Rolling up of the stretched sheets

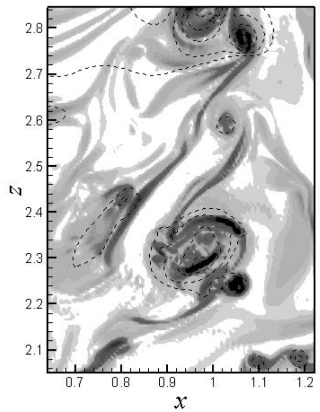

Occurrence of instability cascade

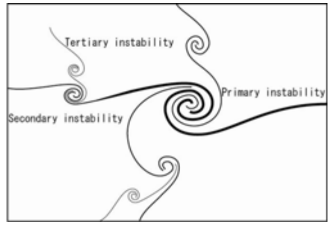

Energy spectrum

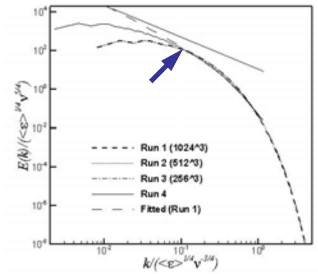

Decomposition of the strain production and vortex-stretching terms in the three regions (t =2.75)

Region	$\frac{\langle -SSS\rangle+\langle \Omega\Omega S\rangle}{\langle -SSS\rangle_t+\langle \Omega\Omega S\rangle_t}$	$\frac{\langle \Omega\Omega S\rangle_t}{\langle -SSS\rangle_t}$	Strain production term fraction	Vortex stretching term fraction
Curved sheet	0.32	0.07	0.39	0.09
Flat sheet	0.41	0.28	0.42	0.36
Tube-core	0.27	0.99	0.18	0.55

Decomposition of turbulence statistics in three regions

Region	Grid point fraction	Energy fraction	Dissipation fraction	Energy individual	Dissipation individual	Taylor micro scale Re
Curved	0.26	0.27	0.33	1.04	0.80	80.5
Flat	0.39	0.38	0.39	1.00	0.65	85.8
Core	0.35	0.34	0.28	0.97	0.50	95.1

Correlation between the vortex sheet and dissipation rate

Isosurfaces of dissipation

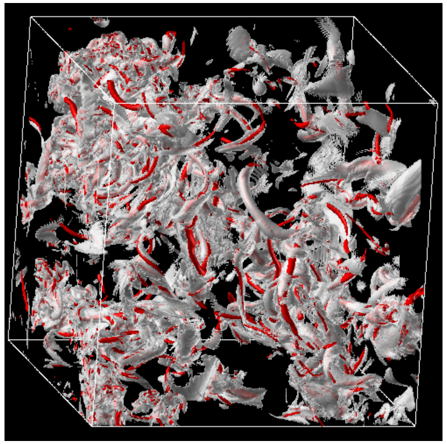

Isosurfaces of vortex sheet

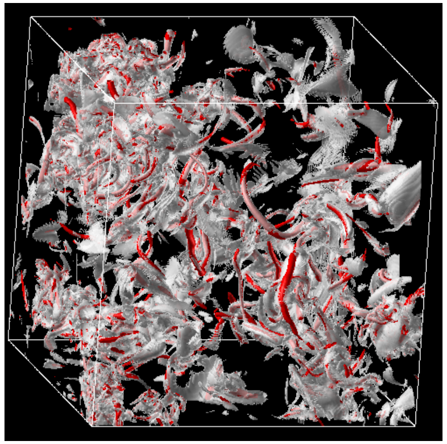

Resolution of spiral turns

Run 2 ($k_{max}\overline{\eta}$ =2.0)

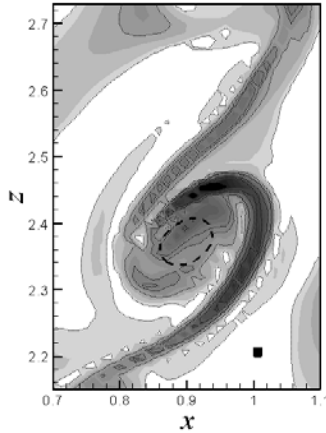

Run 1 ($k_{max}\overline{\eta}$ =4.0)

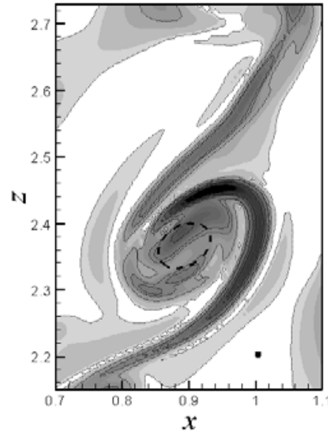

Requirement for the grid point numbers: R_λ^2 is more feasible than $R_\lambda^{3/2}$.

(Sreenivasan 2004)

Formation process of LSV in homogeneous isotropic turbulence

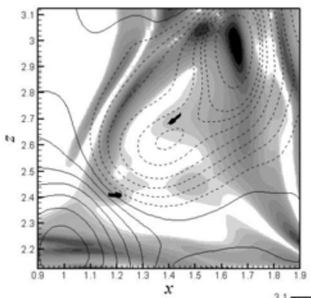

Large scale circulation (lateral extent: comparable to L). Initial configuration is in Mode 3

Mode 3

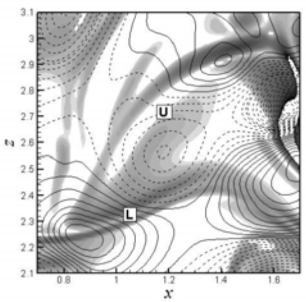

Transformed into Mode 1 or Mode 2.

Mode 1 or 2

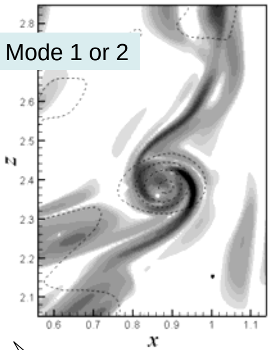

Creation of small scale Mode 1 or Mode 2 LSV.

Horiuti & Fujisawa (2007)

Formation process of spiral vortices in homogeneous isotropic turbulence

Mode 3

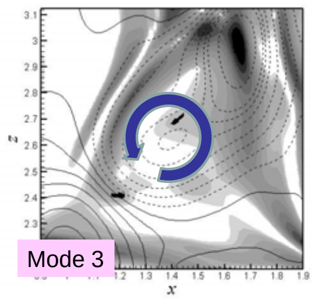

Large scale circulation (lateral extent: comparable to L). Initial configuration is in Mode 3

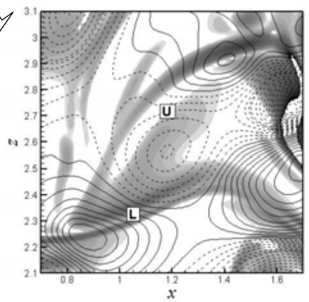

Transformed into Mode 1 or Mode 2.

Mode 1 or 2

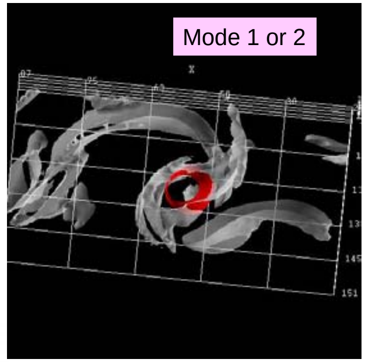

Creation of small scale Mode 1 or Mode 2 LSV.

Horiuti & Fujisawa (2007)

Beltrami decomposition of velocity fields

$u = u^+ + u^-$

Enstrophy (positive helicity) Enstrophy (negative helicity)

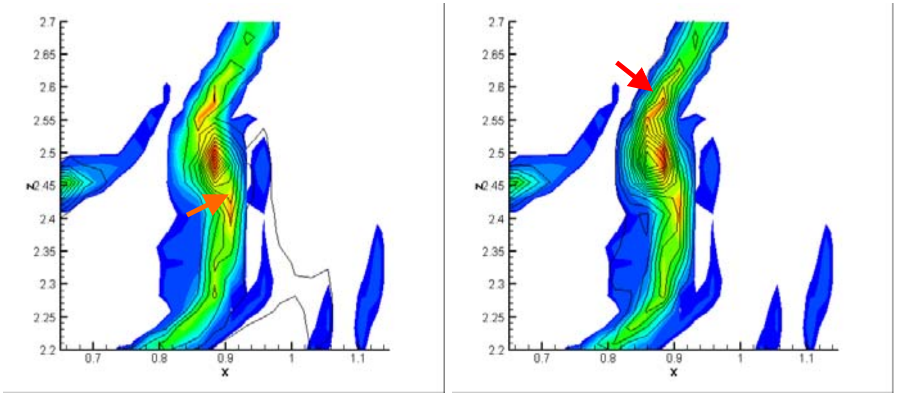

LSV formation at higher Reynolds number

Run 4: Initial velocity field from Run 1 at t=1.75, ν=0.00138 → 0.00024

Vortex-stretching term Run 4 (Re_λ ~ 122.5)

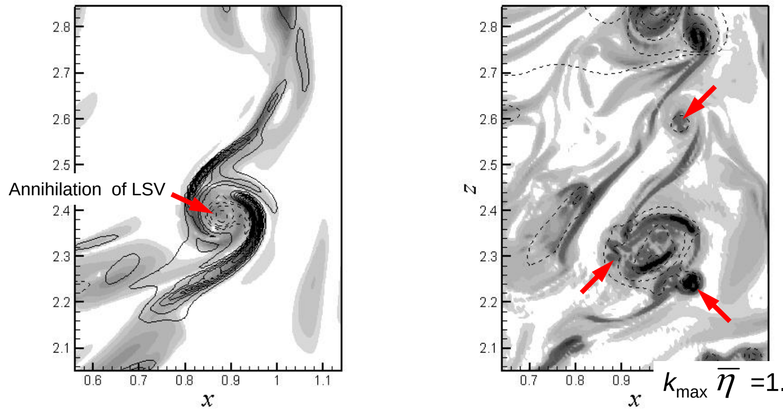

$k_{max}\overline{\eta}$ =1.0

At high Re, the stretched sheets are thinner, and spiral has more turns.

→ Instability of sheets → Creation of extra LSVs along the stretched sheets.

Formation process different from that due to Kelvin-Helmholz instability

Appearance of spiral turns

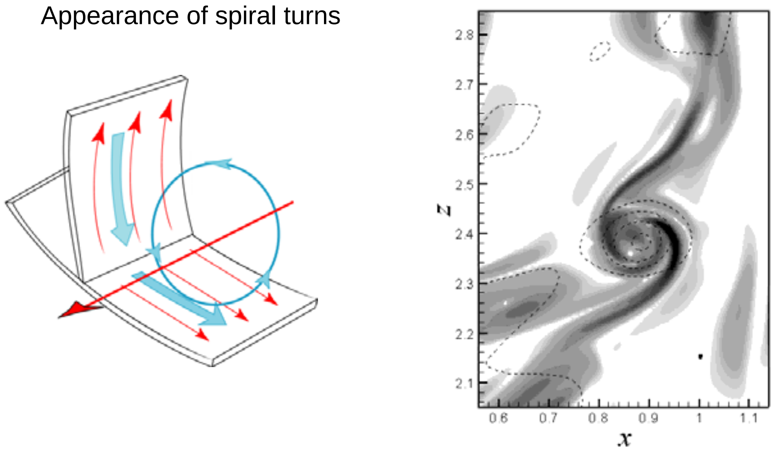

Generation of intense dissipation along the stretched spiral sheets

Inter-mode transition of stretched spiral vortex

Vortex stretching term: $\sigma_z\,\omega_z^{\,2}$

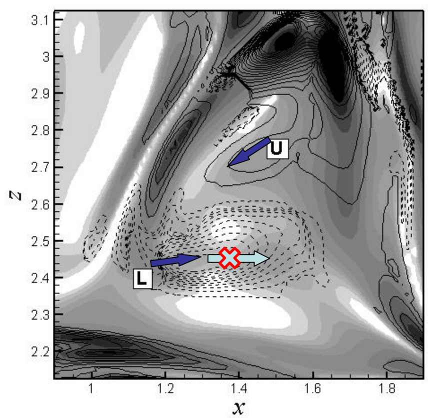

$\omega_z = \boldsymbol{\omega}\cdot\mathbf{e}_z,\ \ \omega_+ = \boldsymbol{\omega}\cdot\mathbf{e}_+,\ \ \omega_- = \boldsymbol{\omega}\cdot\mathbf{e}_-$

Initial configuration: Mode 3
→ Occurrence of reorientation of vorticity direction along lower sheet

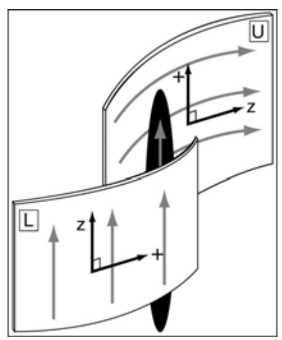

Mode 3 – Mode 2 transition

A process for formation of vortex tube along flat sheet

Strain-rate eigenvalue σ_z (negative)

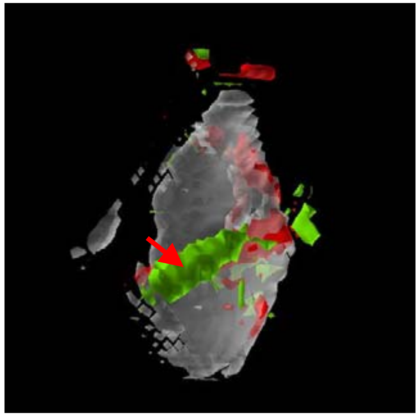

Occurrence of compression in the stretching(z-) direction along the flat sheet.

Distributions of decomposed vortex-stretching terms

Stretching (z) direction (negative)

$\sigma_z\,\omega_z^{\,2}$ (-7500)

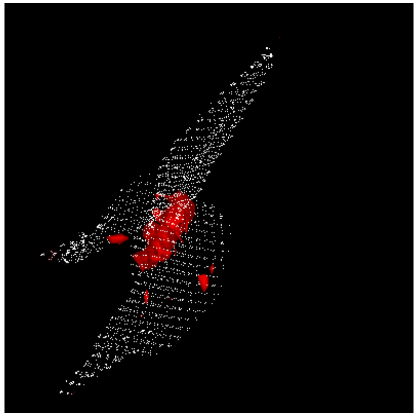

Azimuthal (+) direction (positive)

$\sigma_+\,\omega_+^{\,2}$ (12000)

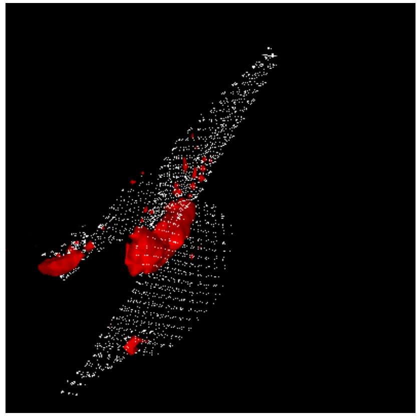

Roles of the pressure for the sheet-tube transformation process

Relaxation of occurrence of compression through the pressure Hessian terms.

Pressure Hessian Π_{++}

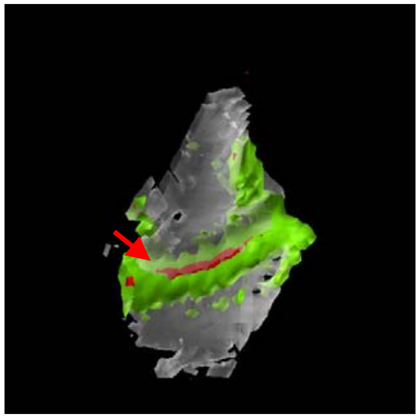

Cross-section of pressure and flat sheet

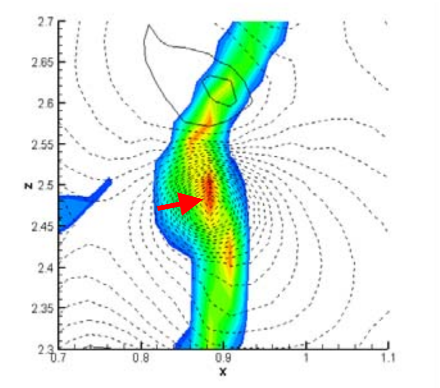

Generation of local minimum pressure ⇒ Formation of the core region of tube
⇒ Generation of vortex tube with transverse vorticity.

Role of the pressure Hessian term for vorticity generation

Governing equations for vorticities, ω_z, , ω_+ , ω_-

$$\begin{cases} \dfrac{D}{Dt}\left(\dfrac{1}{2}\omega_z^2\right) = \sigma_z\omega_z^2 - \dfrac{1}{4}\dfrac{\omega_z\omega_+}{\sigma_z-\sigma_+}\tilde{\Pi}_{z+} & <0 \\ \dfrac{D}{Dt}\left(\dfrac{1}{2}\omega_+^2\right) = \sigma_+\omega_+^2 + \dfrac{1}{4}\dfrac{\omega_+\omega_z}{\sigma_z-\sigma_+}\tilde{\Pi}_{+z} & >0 \end{cases}$$

$$\omega_z\omega_+\tilde{\Pi}_{z+} < 0 \quad \therefore \frac{\omega_z\omega_+}{\sigma_z-\sigma_+}\tilde{\Pi}_{z+} > 0$$

$$\Downarrow$$

$$\omega_z^2 \searrow \;,\; \omega_+^2 \nearrow$$

$\omega_z\omega_+\Pi_{z+}$ (negative)

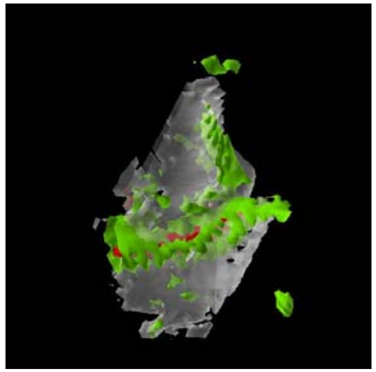

Pressure Hessian term reacts to relax an occurrence of compression in z-dir.
by converting the ω_z vorticity into the transverse component, ω_+.

Statistical measure for frequency of occurrence of mode transitions

$\widetilde{\Pi}_{zz}$ (Conditionally sampled in the sheet region) p.d.f. of $\sigma_z\omega_z^2$

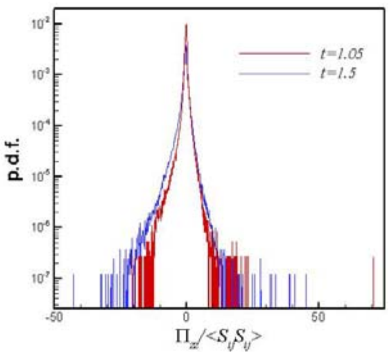

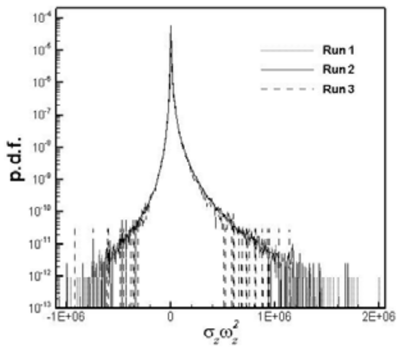

At an early stage: skewed to positive values
→ Occurrence of reorientation of vorticity direction
At a later time: skewed to negative values
→ The vorticity in the converted direction grows.

Appearance of a markedly large proportion of negative $\sigma_z\omega_z^2$
→ Occurrence of reorientation of vorticity direction

Inter-component energy exchange in Mode 2

Governing equations for energy: u_z^2, u_+^2

$$\begin{cases} \dfrac{D}{Dt}\left(\dfrac{1}{2}u_z^2\right) = -\dfrac{1}{4}\dfrac{u_z u_+}{\sigma_z-\sigma_+}\left(\omega_z\omega_+ - \widetilde{\Pi}_{z+}\right) \\ \dfrac{D}{Dt}\left(\dfrac{1}{2}u_+^2\right) = +\dfrac{1}{4}\dfrac{u_z u_+}{\sigma_z-\sigma_+}\left(\omega_z\omega_+ - \widetilde{\Pi}_{z+}\right) \end{cases}$$

$$-\frac{1}{4}\frac{u_z u_+}{\sigma_z-\sigma_+}\left(\omega_z\omega_+ - \widetilde{\Pi}_{z+}\right) < 0, \quad \left(\sigma_z - \sigma_+ < 0\right)$$

⇩ on upper sheet

$u_z^2 \searrow, \quad u_+^2 \nearrow$

$-\frac{1}{4}u_z u_+ \omega_z \omega_+$

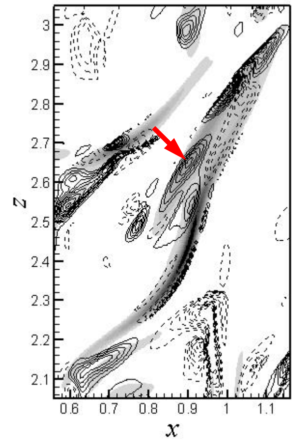

Energy transfer from the z-component, u_z^2, to the transverse component, u_+^2.

Mode 1 LSV is more persistent than Mode 2 LSV.

Correlation between the vortex sheet and dissipation rate

Isosurfaces of dissipation

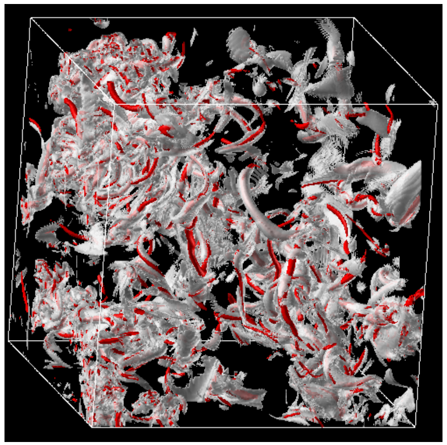

Isosurfaces of vortex sheet

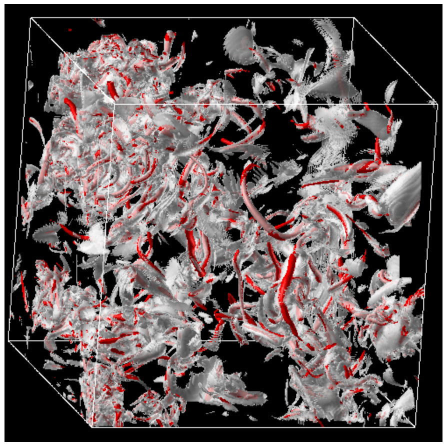

Resolution of spiral turns

Run 2 ($k_{max}\overline{\eta}$ =2.0)

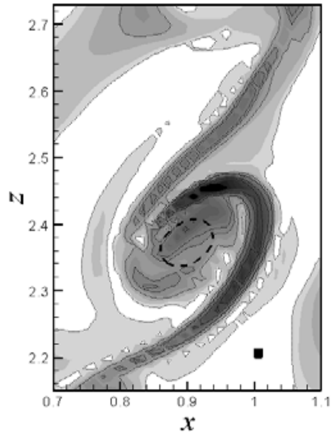

Run 1 ($k_{max}\overline{\eta}$ =4.0)

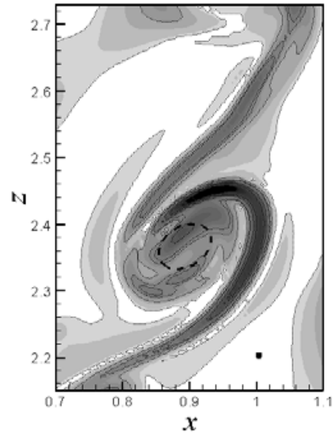

Requirement for the grid point numbers: R_λ^2 is more feasible than $R_\lambda^{3/2}$.

(Sreenivasan 2004)

LSV formation at higher Reynolds number

Run 4: Initial velocity field from Run 1 at t=1.75, ν=0.00138 → 0.00024

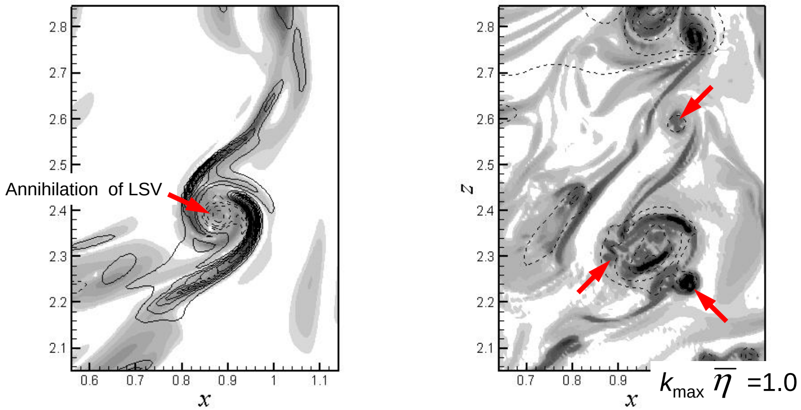

At high Re, the stretched sheets are thinner, and spiral has more turns.

→ Instability of sheets → Creation of extra LSVs along the stretched sheets.

LSV formation at higher Reynolds number

Run 4: Initial velocity field from Run 1 at t=1.75, ν=0.00138 → 0.00024

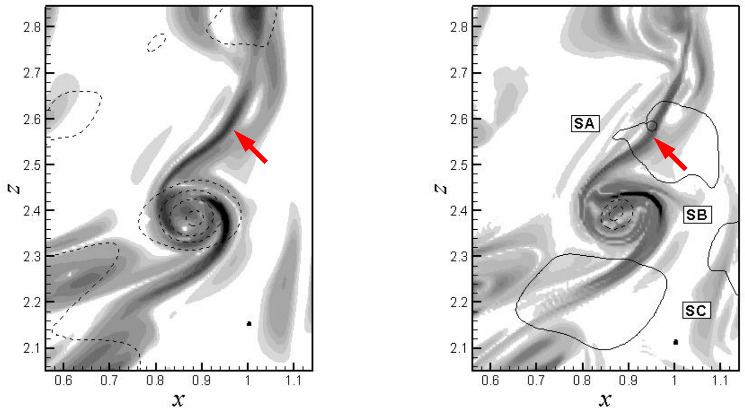

At high Re, the stretched sheets are thinner, and spiral has more turns.
⇒ Instability of sheets ⇒ Creation of extra LSVs along the stretched sheets.

Inter-mode transition of stretched spiral vortex in forced turbulence

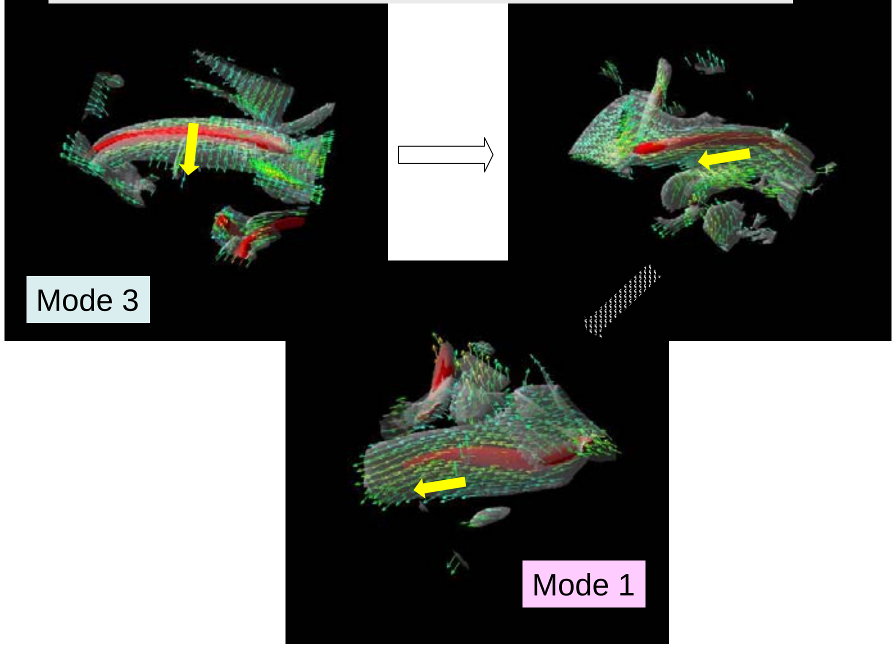

Topological transformation: helicity $h = u \cdot \omega$

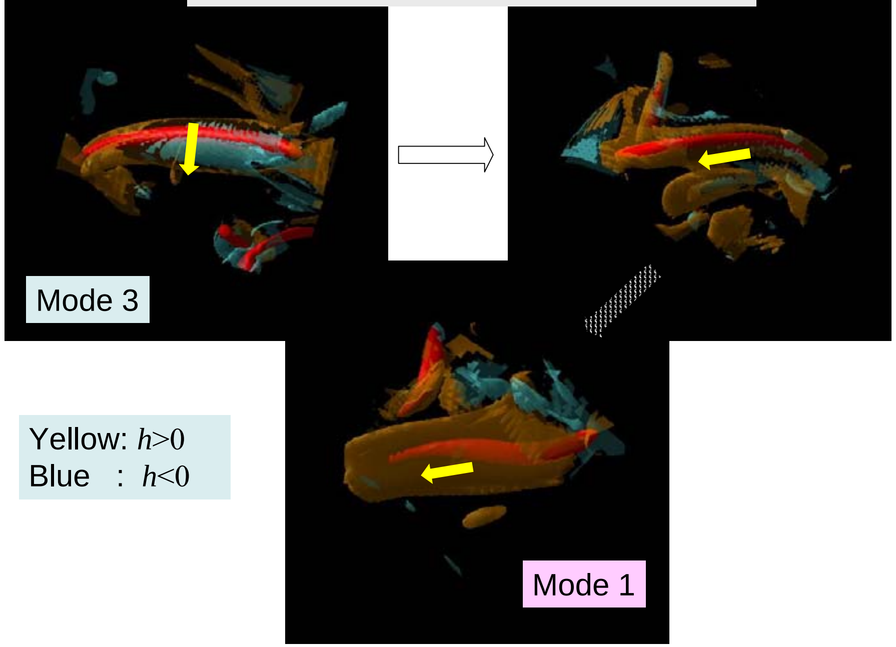

Topological transformation: helicity production term P_h

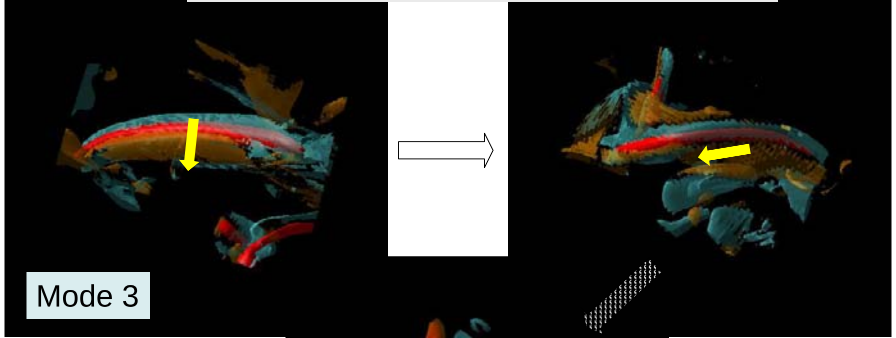

Represented by

$$\frac{Dh}{Dt} = -\left[\frac{\partial}{\partial x_i}\left(p - \frac{1}{2}u_k u_k\right)\right]\cdot \omega_i$$
$$\equiv -P_h$$

(Holm & Kerr 2002)

Yellow: $h>0$
Blue : $h<0$

295500step
Q=500
Heli+:黄色
Heli-:水色

295500step
Q=500
H+:黄色
H-:水色

296000step
Q=500
Heli+:黄色
Heli-:水色

296000step
Q=500
H+:黄色
H-:水色

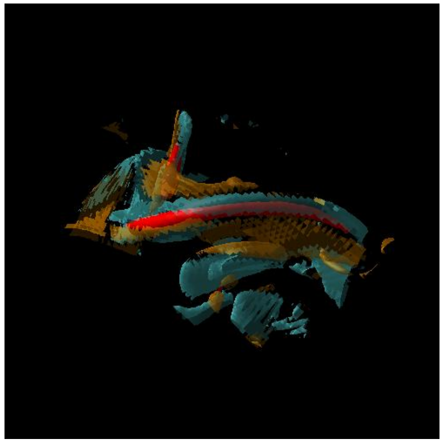

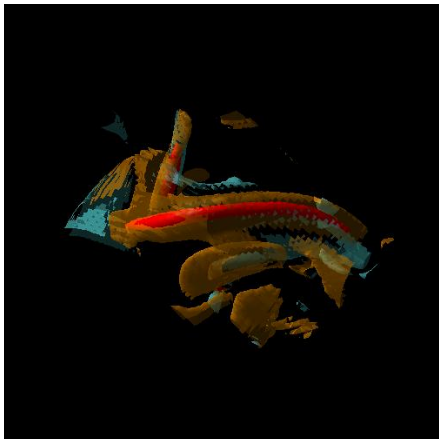

296500step
Q=500
Heli+:黄色
Heli-:水色

296500step
Q=500
H+:黄色
H-:水色

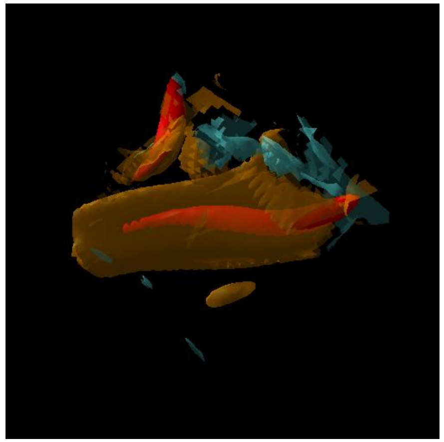

296500step
Q=500
Heli+:黄色
Heli-:水色

296500step
Q=500
H+:黄色
H-:水色

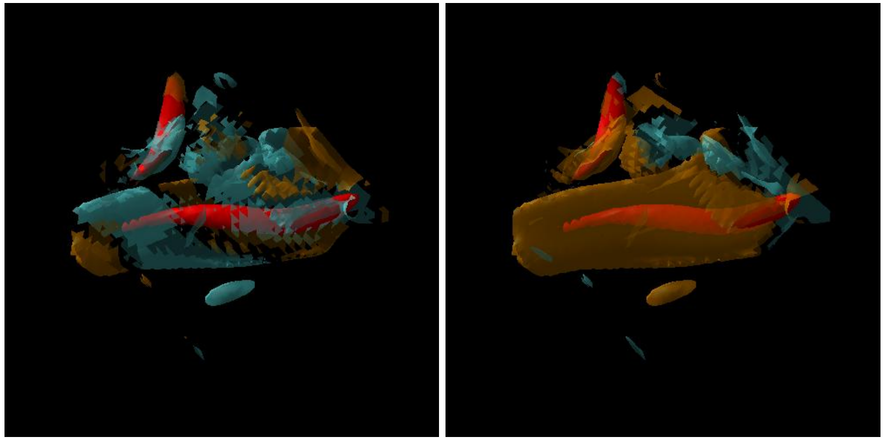

Hierarchical spectrum and multi-mode spiral vortex

$$E(k) \approx K_0 \varepsilon^{2/3} k^{-5/3} + C_1 \dot{\varepsilon} \varepsilon^{-2/3} k^{-7/3}$$

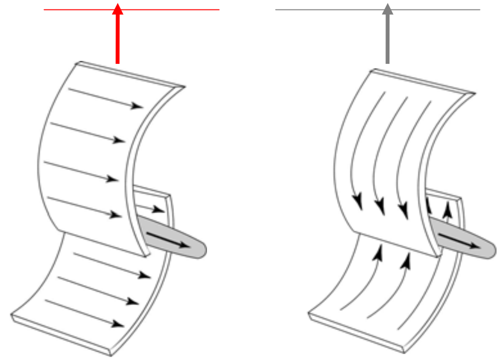

Spiral vortex in Mode 1　　Mode 3

Mode 2: intermediate between -5/3 and -7/3

Derivation of -7/3 energy spectrum (1)

Pullin and Lundgren (2001):

$$E(k) = \frac{1}{\Gamma\left(2/3\right)}\left(2/3\right)^{\frac{2}{3}} \frac{\varepsilon}{\nu^{\frac{1}{3}} a^{\frac{2}{3}}} k^{-\frac{5}{3}} + \frac{1}{\Gamma\left(1/3\right)}\left(2/3\right)^{\frac{1}{3}} \frac{\varepsilon}{\nu^{\frac{2}{3}} a^{\frac{1}{3}}} k^{-\frac{7}{3}}$$

Define the stretching parameter a using the Kolmogorov scaling: $a = \left(\frac{\varepsilon}{15\nu}\right)^{\frac{1}{2}}$

$$E(k) = \frac{1}{\Gamma\left(2/3\right)}\left(20/3\right)^{\frac{1}{3}} \varepsilon^{\frac{2}{3}} k^{-\frac{5}{3}} + \frac{1}{\Gamma\left(1/3\right)}\left(2/3\right)^{\frac{1}{3}} 15^{\frac{1}{6}} \nu^{-\frac{1}{2}} \varepsilon^{\frac{5}{6}} k^{-\frac{7}{3}}$$

Diverge as $\nu \longrightarrow 0$ unless $\varepsilon \longrightarrow 0$.

Removal of divergence by using a large scale shear rate, S.

$$E(k) \sim \varepsilon^{1/3} S\, k^{-7/3} \qquad \left(a \approx \left(\frac{\varepsilon}{\nu}\right)^{2} S^{-3} \right)$$

$E_{12}(k) \sim \varepsilon^{1/3} S\, k^{-7/3}$
(Ishihara *et al.* 2002)

Derivation of -7/3 energy spectrum (2)

Cascade picture for the evolution of the vorticity blob (Gilbert 1993)

- Stretching of axial vorticity ω_z $\rightarrow$ $E(k) \propto k^{-5/3}$
- Stretching of azimuthal vorticity ω_θ $\rightarrow \propto k^{-7/3}$ (Ohkitani 2004)
- Stretching of azimuthal vorticity ω_r $\rightarrow \propto k^{-9/3}$

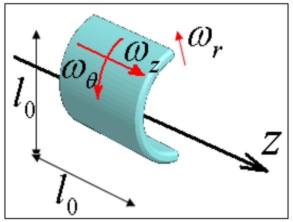

Enstrophy spectrum:

$$\Omega(k) \approx (l_0^{\,11} \omega_0^{\,10} / a^7)^{1/3} k^{-1/3}$$

$$\dot{K} = -\varepsilon \quad \Rightarrow \quad \dot{\varepsilon} \approx -\frac{\varepsilon^2}{K}$$

$$\left(\frac{l_0^{\,11} \omega_0^{\,10}}{a^7}\right)^{1/3} \approx \frac{\varepsilon^2}{K} \varepsilon^{-2/3} \approx \dot{\varepsilon} \varepsilon^{-2/3}$$

$$E(k) \propto \dot{\varepsilon} \varepsilon^{-2/3} k^{-7/3}$$

K: turbulent energy
$\dot{\varepsilon}$: Time derivative of ε

Phase 1 ⇒ Phase 2

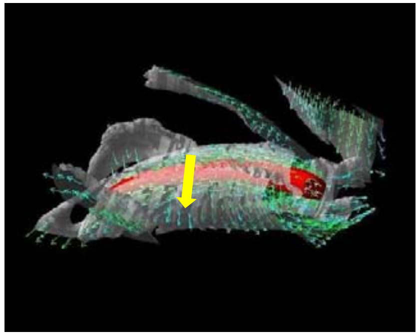

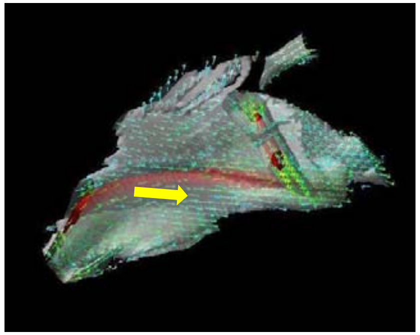

Mode 3 ⇒ Mode 1

- Mode 3 (or 2) tends to be converted to Mode 1 (Horiuti *et al.* 2008)
- Rolling-up of the stretched sheet ⇒ Creation of Mode 1 spiral vortices

⇒ Mode 1 spiral vortex predominates in Phase 2.

Time variations of energy and dissipation rate

Mode 3 d isotropic turbulence

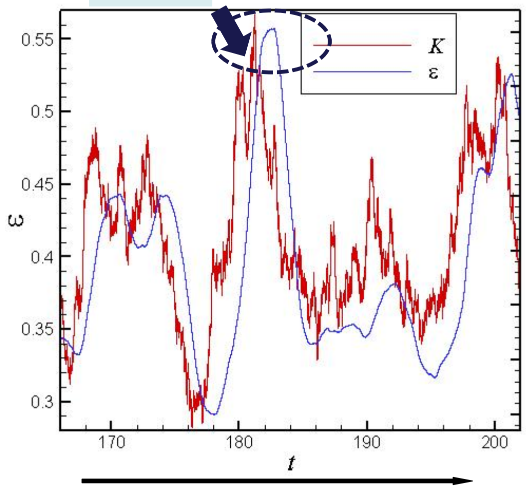

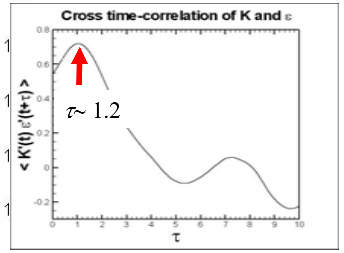

Time lag ~ Cascade time scale ~ Eddy turnover time according to integral scale L (Wan, Xiao, Meneveau *et al*. 2010)

Period of oscillation ~ Eddy turnover time due to forcing: T

Conditional sampling of energy spectrum

<u>Extracted spectra</u>

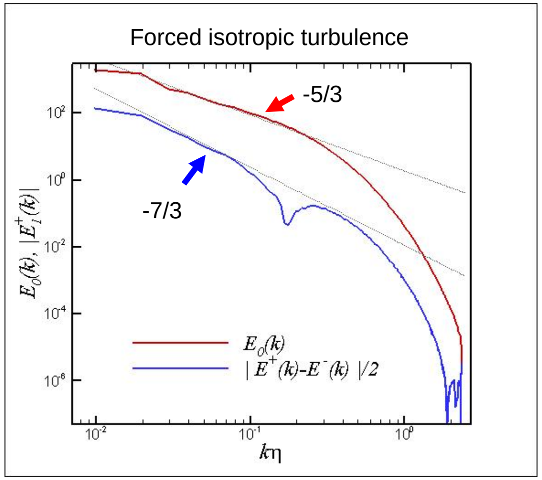

C_K ~ 1.61
C_1 ~ C_K
Heisenburg: C_1~ 3/7C_K

Energy flux and transfer function: Average in Phases 1 and 2

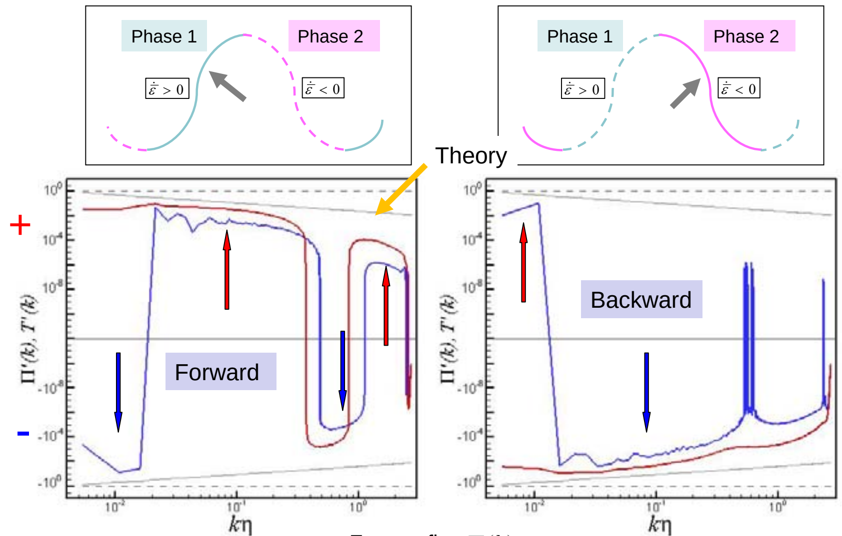

Energy flux $\Pi(k)$
Transfer function $T(k)$

Flux and transfer function: Average in Phase T

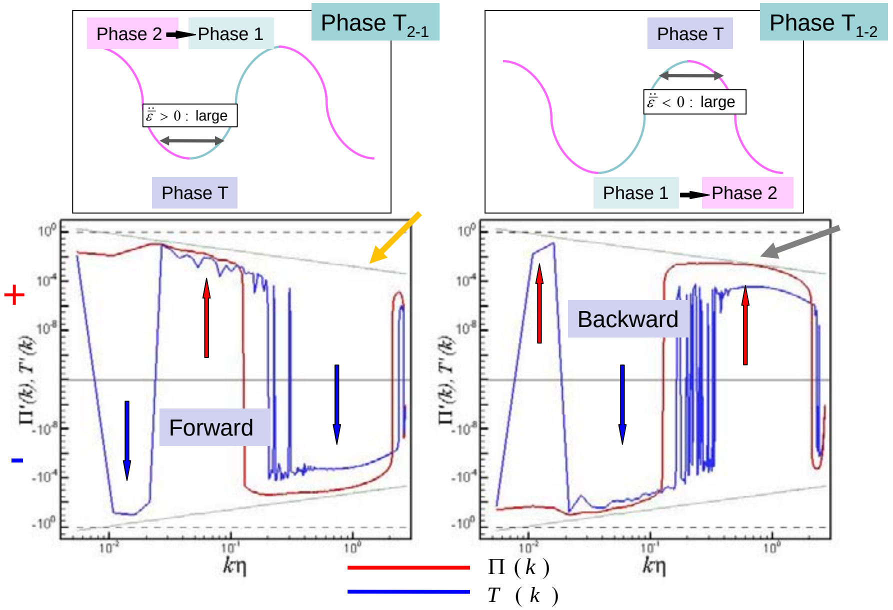

Conditional sampling of energy spectrum

Extracted spectra

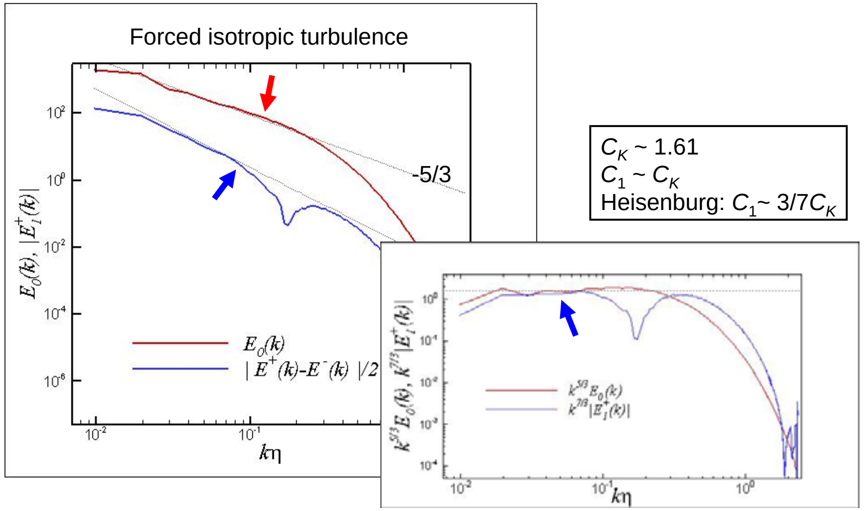

$C_K \sim 1.61$
$C_1 \sim C_K$
Heisenburg: $C_1 \sim 3/7C_K$

Extraction of the non-equilibrium spectrum

1. Random forcing

Grid points	1024^3
$k_{max}\,\eta$	2.49
R_λ	243.3
$<K>$	1.43

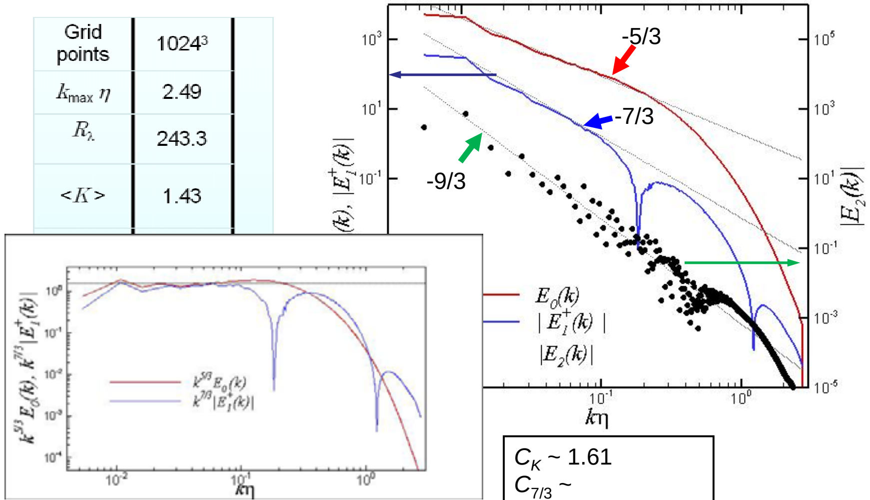

$C_K \sim 1.61$
$C_{7/3} \sim 2C_K^2/3=1.73$

Non-equilibrium energy spectrum (Kovasnay model)

$$E(k)\approx C_K\varepsilon^{2/3}k^{-5/3}+\frac{2}{3}C_K^{\,2}\,\dot{\varepsilon}\,\varepsilon^{-2/3}\underline{k^{-7/3}}+\frac{1}{3}C_K^{\,3}\left[\ddot{\varepsilon}\,\varepsilon^{-1}-(\dot{\varepsilon})^2\varepsilon^{-2}\right]\underline{k^{-9/3}}+\cdots$$

$$=C_K\varepsilon^{2/3}k^{-5/3}+\frac{2}{3}C_K^{\,2}\frac{d(\log\varepsilon)}{dt}\varepsilon^{1/3}k^{-7/3}+\frac{1}{3}C_K^{\,3}\frac{d^2(\log\varepsilon)}{dt^2}k^{-9/3}+\cdots$$

➡ Long-time average of the spectrum: $\langle E(k)\rangle = C_k\varepsilon^{2/3}k^{-5/3}$

Objective

- Extract the $k^{-7/3}$ and $k^{-9/3}$ spectrum using conditional sampling of the spectrum in quasi-steady turbulence DNS data.
- Discuss on the effect of non-locality in the transfer function.
- Elucidate the roles of the $k^{-7/3}$ and $k^{-9/3}$ spectrum in generation of energy transfer and examine the non-equilibrium/unsteady effect.

Multi-mode stretched spiral vortex

Topological classification with regards to vorticity alignment along the two sheets and the tube

3-dimensional rendering

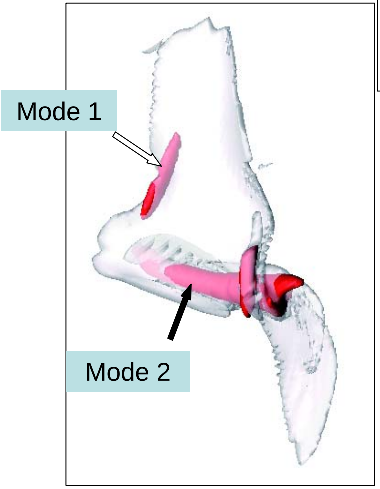

Horiuti & Fujisawa (2008)

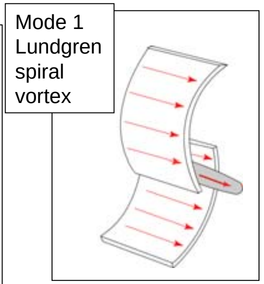

$k^{-5/3}$ spectrum

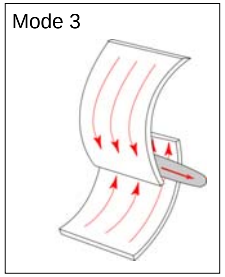

$k^{-7/3}$ spectrum

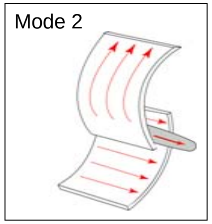

Intermediate

Multi-mode stretched spiral vortex

Topological classification with regards to vorticity alignment along the two sheets and the tube

3-dimensional rendering

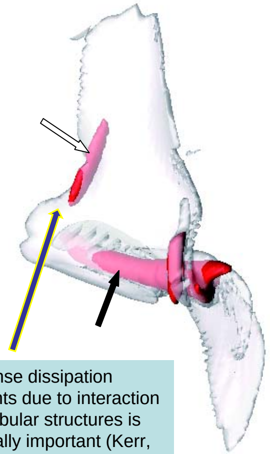

Intense dissipation events due to interaction of tubular structures is equally important (Kerr, Goto, IMS6)

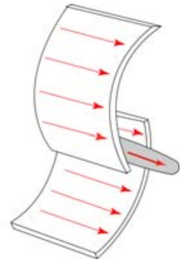

Mode 1
(Lundgren 1982)

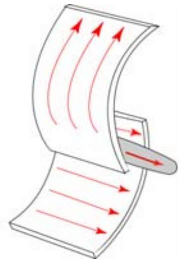

Mode 2

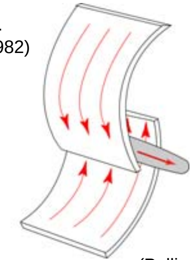

Mode 3
(Pullin & Lundgren 2003)

Possibility in reduction of turbulence generation by means of termination of the occurrence of LSV formation

Tom's effect : Drag reduction in the polymer-diluted flows

Investigation of the effect of viscoelasticity on the formation process

Characteristic features of the viscoelastic fluids

1. Inhibition of the vortex generation.
2. Normal stress difference (appearance of elongational viscosity).
3. Shear-rate dependent viscosity (shear thinning).

How these viscoelastic features affect the LSV formation process.

Weissenburg effect (Rod clibming)

a dilute solutionof polystyrene polymer is dissolved in newtonian solvent (Piccolastic).
(HP: Prof. McKinley, MIT)

Characteristic features of the viscoelastic fluids

1. Inhibition of the vortex generation.
2. Normal stress difference (appearance of elongation rate and viscosity).
3. Shear-rate dependent viscosity (shear thinning).

Weissenburg effect
(Rod clibming)

In this video clip a dilute (0.025 wt%) solution of a high molecular weight (2ק10⁶ g/mol) polystyrene polymer (Polysciences Inc) is dissolved in a low molecular weight (~100 g/mol) newtonian viscous (~30 Pa.s) solvent (Piccolastic, Hercules Inc).
In the experiment a rod is rotated with its end immersed in the fluid outlined above. In the Newtonian case inertia would dominate and the fluid would move to the edges of the container, away from the rod. Here however the elastic forces generated by the rotation of the rod (and the consequent stretching of the polymer chains in solution) result in a positive normal force - the fluid rises up the rod. The bulbous shape remaining at the end of the video is the onset of instability as the mass that has been forced up the rod a) relaxes and b) overcomes the force pushing from below.

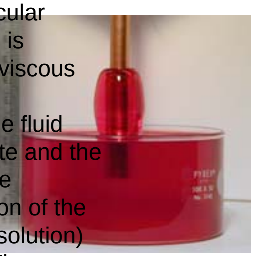

a dilute solutionof polystyrene polymer is dissolved in newtonian solvent (Piccolastic).

How these viscoelastic features affect on the occurrence of sheet-tube transformation process.

Incorporation of non-affine effect into the constitutive equation

Assumption of complete affinity

$$\dot{\boldsymbol{Q}} = \boldsymbol{Q} \cdot \nabla \boldsymbol{u}$$

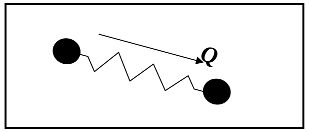

< Elastic dumbbell >

$\boldsymbol{Q}$: connector vector

$$\frac{D}{Dt}\langle Q_i Q_j \rangle = \langle Q_i Q_k \rangle \frac{\partial u_j}{\partial x_k}$$

⇒ Upper-convective Oldroyd-B constitutive equation

Introduction of non-affinity

$$\dot{\boldsymbol{Q}} = \boldsymbol{Q} \cdot [\nabla \boldsymbol{u} - 2\alpha \boldsymbol{S}] \qquad (\alpha : \text{slip parameter}, 0 \le \alpha \le 1)$$

⇒ Johnson-Segalman constitutive equation

Governing equation for motion of viscoelastic fluid

$$\frac{\partial u_i}{\partial t} + \frac{\partial (u_i u_j)}{\partial x_j} = -\frac{\partial p}{\partial x_i} + \beta \nu \frac{\partial^2 u_i}{\partial x_j \partial x_j} - \frac{\partial \tau_{ij}}{\partial x_j}$$

Constitutive equation for the polymer stress tensor τ_{ij}

Johnson-Segalman constitutive equation (JS model)

$$\frac{D\tau_{ij}}{Dt} = (1-\alpha)\left(\tau_{ik}\frac{\partial u_j}{\partial x_k} + \frac{\partial u_i}{\partial x_k}\tau_{kj}\right) - \alpha\left(\tau_{ik}\frac{\partial u_k}{\partial x_j} + \frac{\partial u_k}{\partial x_i}\tau_{kj}\right)$$
$$-\frac{1}{\lambda}\tau_{ij} - \frac{\nu(1-\beta)}{\lambda}2S_{ij} + \kappa\frac{\partial^2 \tau_{ij}}{\partial x_k \partial x_k}$$

Cf. Vaithianathan et al. (2006)

Introduction of non-affinity

$\boldsymbol{Q}$: connector vector

$$\dot{\boldsymbol{Q}} = \boldsymbol{Q} \cdot \nabla \boldsymbol{u} \Rightarrow \dot{\boldsymbol{Q}} = \boldsymbol{Q} \cdot [\nabla \boldsymbol{u} - 2\alpha \boldsymbol{S}]$$

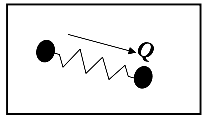

α : slip parameter

α=0: reduced to Oldroyd-B eq. (Review in Procaccia & Sreenivasan 2008)
α=1: reduced to Oldroyd-A eq.

Parameters of the viscoelastic homogeneous-isotropic DNS data

- Grid point numbers: 128^3
- Molecular discosity : ν=0.004
- Polymer relaxation time : λ =0.45 (Taylor: 0.66, Kolmogorov: 0.098)
- Non-affine slip parameter: α=0.0, 0.5, 1.0
- Solvent viscosity contribution: β=0.8
- Artificial viscosity: $\kappa = 0.05$
- External forcing: Random phase with an energy spectrum

$$E_f(k,t) = \begin{cases} C_f, (1.0 \le k \le 2.5) \\ 0, \quad \textit{otherwise} \end{cases}$$

- Initial condition: Newtonian steady turbulence ($R_\lambda \sim 90.0$)
- No damping function for the polymer stress is employed
- Work provided by the forcing to sustain the steady state

$\langle u_i f_i \rangle$		
Newtonian	α=0.0	α=1.0
0.470	> 0.468	> 0.457

Temporal development of vortex sheets and tubes (Newtonian)

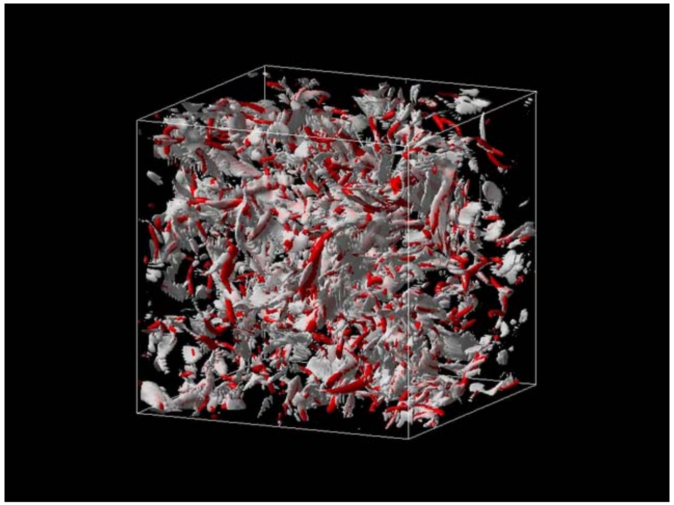

Temporal development of vortex sheets and tubes (viscoelastic)

α=0.0 α=1.0

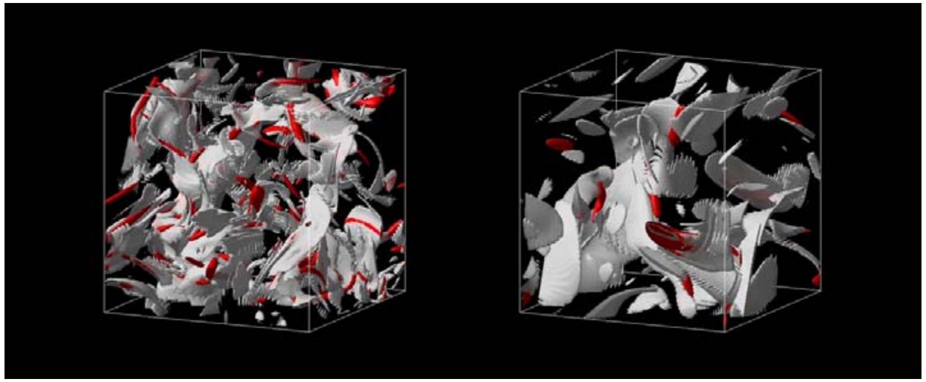

Temporal development of vortex sheets and tubes (viscoelastic)

α=0.0 α=1.0

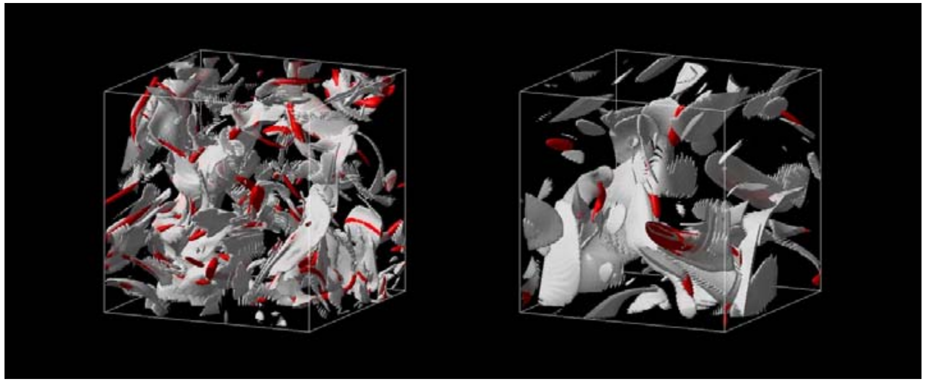

Characteristic features of the viscoelastic fluids

Weissenburg effect

Governing equation for radial momentum

$$r\frac{d}{dr}\left(p-\tau_{zz}\right)=r\frac{d}{dr}\left(\tau_{rr}-\tau_{zz}\right)+\underline{\left(\tau_{rr}-\tau_{\theta\theta}\right)}+\cdots$$

R. Bird *et al.* "Dynamics of Polymeric Liquids" vol.1 (1987)

Determination of normal stress difference is required.

Polymer stress on the basis of $[A_{ij}]$ eigenvectors along the tube

a_+: in the radial direction a_-: in the azimuthal direction a_s: in the longitudinal direction

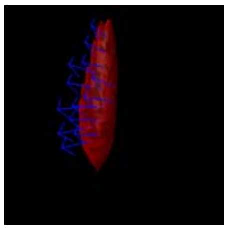

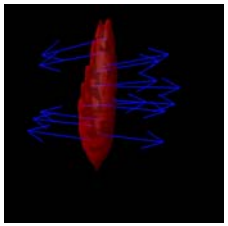

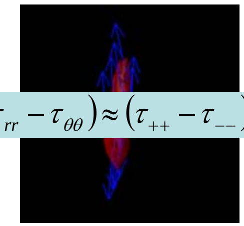

$$\left(\tau_{rr}-\tau_{\theta\theta}\right)\approx\left(\tau_{++}-\tau_{--}\right)$$

Roles of normal stress difference on the vortex tube generation

$$\left(\tau_{rr}-\tau_{\theta\theta}\right)\approx\left(\tau_{++}-\tau_{--}\right)$$

Pressure gradient in the radial direction

$$r\frac{d}{dr}\left(p-\tau_{zz}\right)=r\frac{d}{dr}\left(\tau_{rr}-\tau_{zz}\right)+\underline{\left(\tau_{rr}-\tau_{\theta\theta}\right)}+\cdots$$

Distribution of $\left(\tau_{++}-\tau_{--}\right)$ on the tube

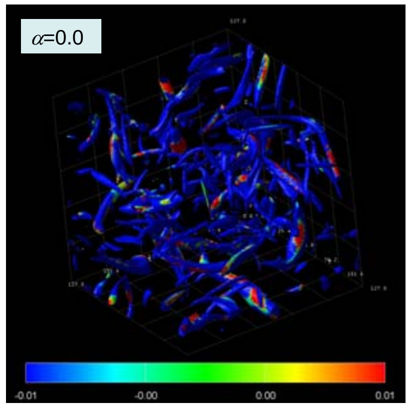

$\left(\tau_{++}-\tau_{--}\right)$: predominantly negative

$$\therefore \frac{dp}{dr}<0$$

Pressure bulges out in tube core region
⇒ Reduction of lowering of pressure in the tube core.
⇒ Reduction of growth of the tube.

Inhibition of the vortex generation

Effect of viscoelasticity on the pressure force

Decomposition of the pressure into those due to solvent p_s and polymer p_τ

$$\Delta p_s = 2Q, \qquad \Delta p_\tau = -\frac{\partial}{\partial x_i}\left(\frac{\partial \tau_{ij}}{\partial x_j}\right) \equiv -T$$

Joint pdf of source terms Q and T

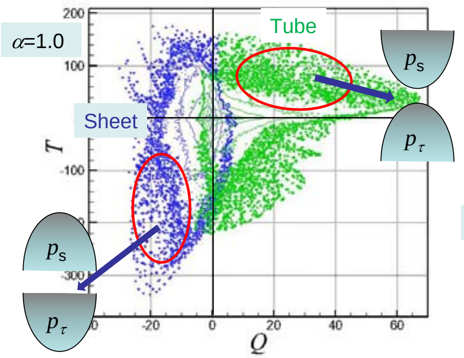

PDF of angle between ∇p_s and ∇p_τ

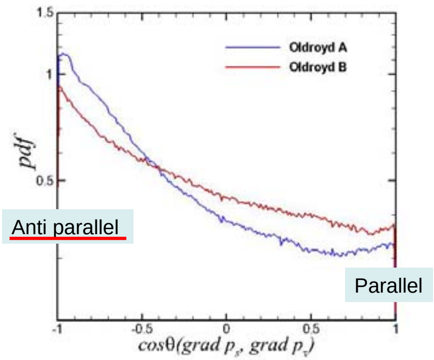

∇p_τ tends to oppose to ∇p_s ⇒ Reduction of stretching of tube and sheet

Determination of normal stress difference along the sheet

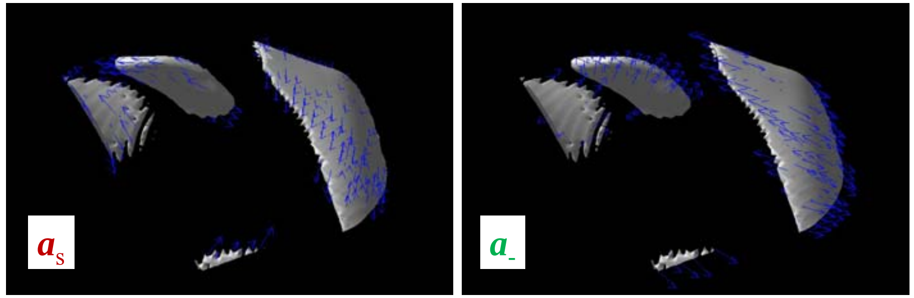

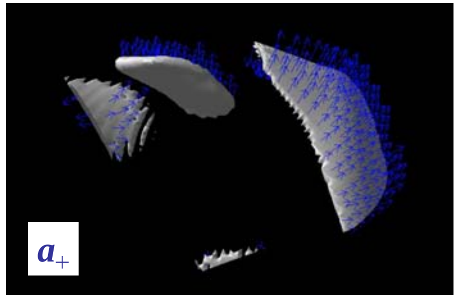

Alignment of $[A_{ij}]_+$ eigenvectors with vortex sheet

a_+ eigenvector is mostly perpendicular to the vortex sheet.

Vortex sheet is approximately spanned by the a_s and a_- eigenvectors.

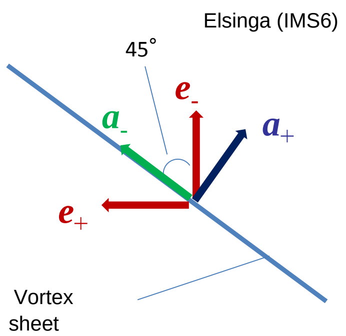

First and second normal stress differences along the vortex sheet

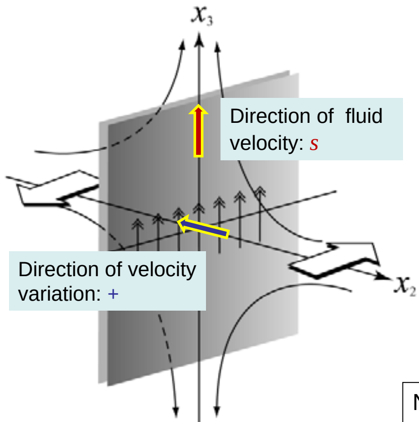

First normal stress difference

$$(\tau_{11} - \tau_{22}) \approx (\tau_{ss} - \tau_{++})$$

Second normal stress difference

$$(\tau_{22} - \tau_{33}) \approx (\tau_{++} - \tau_{--})$$

Note: When the vorticity of sheet is large

⇒ First normal stress difference

$$(\tau_{11} - \tau_{22}) \approx (\tau_{--} - \tau_{++})$$

⇒ Second normal stress difference

$$(\tau_{22} - \tau_{33}) \approx (\tau_{++} - \tau_{ss})$$

First and second normal stress differences along the vortex sheet

First: $(\tau_{11}-\tau_{22})\approx(\tau_{ss}-\tau_{++})$ Second: $(\tau_{22}-\tau_{33})\approx(\tau_{++}-\tau_{--})$

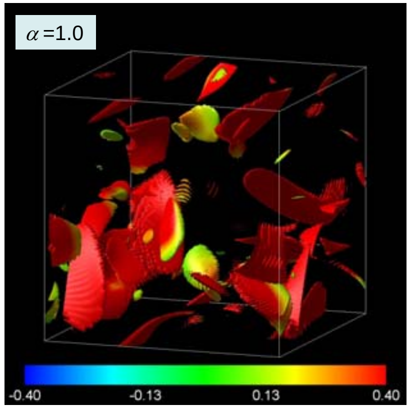

Predominantly positive

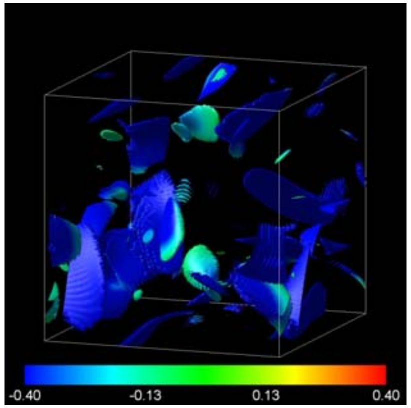

Predominantly negative

Stretching and alignment of the polymer molecules along the streamlines ⇒

⇒ Extra tension exerted along the sheet ⇒ Snap back of the sheet to the original form

Elongational (or extensional) viscosity

The most likely reason for drag reduction:

Enhanced extensional viscosity leads to increased resistance to extensional motions of the turbulent flow (Lumley 1969)

Toonder *et al.* (1995) Strain parameter to identify occurrence of elongation
Sureshkumar *et al.* (1997) the maximum polymer extension L in FENE-P model

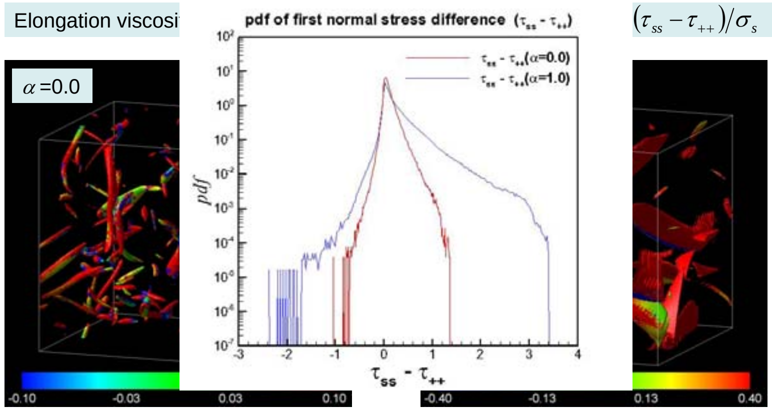

Effect of viscoelasticity on the occurrence of a role reversal between the eigenvalues

$$\frac{DS_{ij}}{Dt}=-\frac{1}{2}\left(\frac{\partial u_k}{\partial x_j}\frac{\partial u_i}{\partial x_k}+\frac{\partial u_k}{\partial x_i}\frac{\partial u_j}{\partial x_k}\right)-\Pi_{ij}-\frac{1}{2}\mathrm{T}_{ij}$$

$$\mathrm{T}_{ij}=\frac{\partial^2\tau_{ik}}{\partial x_j\partial x_k}+\frac{\partial^2\tau_{jk}}{\partial x_i\partial x_k}$$

$$\mathrm{T}=\mathrm{E}^{\mathrm{T}}(\mathrm{T}_{ij})\mathrm{E},\quad \mathrm{E}=(e_+,e_-,e_z)$$

Off-diagonal component of pressure Hessian

$$\frac{De_+}{Dt}\bullet e_z=\frac{1}{(\sigma_+-\sigma_z)}\left\{-\Pi_{+z}-\frac{1}{2}\mathrm{T}_{+z}\right\}$$

The rate of rotation in the plane defined by $\boldsymbol{e}_+$ and $\boldsymbol{e}_z$ (Nomura & Post 1998)

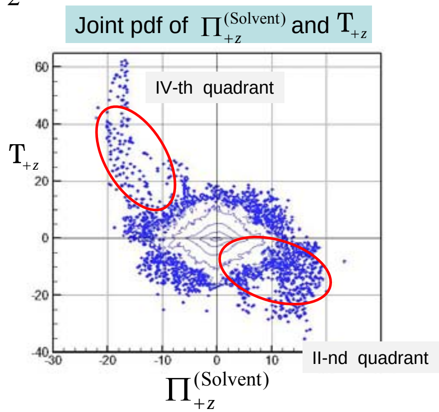

The occurrence of a role reversal is inhibited by the polymer stress

Computed cases in pipe flow DNS

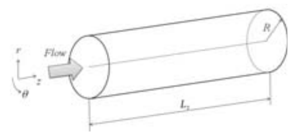

	Newtonian	Johnson-Segalman model
α	—	0.0, 0.1, 0.5, 0.9, 1.0
$\mathrm{Re}_{\tau 0}$	180 $(\mathrm{Re}_{b0}\approx 5300)$	180
$\mathrm{We}_{\tau 0}$	—	25
Domain	$10R\times R\times 2\pi R$	$20R\times R\times 2\pi R$
L_z^+	1,800	3,600
Grid	$128\times 64\times 64$	$256\times 64\times 64$
β	1.0	0.9
$\Delta t u_\tau/R$	2.0×10^{-4}	2.0×10^{-5}

$$\mathrm{Re}_{\tau 0}=\frac{u_\tau R}{\nu_0}$$

$$\mathrm{We}_{\tau 0}=\frac{\lambda u_\tau^2}{\nu_0}$$

Peterlin damping function (FENE-P)

$$f(\tau)=\frac{L^2}{L^2-3}+\frac{\mathrm{We}_{\tau 0}}{\mathrm{Re}_{\tau 0}}\frac{1}{L^2}\left|(1-2\alpha)\tau_{kk}\right|$$

支配方程式

Governing Equations

連続の式 $$\frac{\partial u_i}{\partial x_i}=0$$

運動方程式 $$\frac{\partial u_i}{\partial t}+\frac{\partial (u_i u_j)}{\partial x_j}=-\frac{\partial p}{\partial x_i}+\frac{\beta}{\mathrm{Re}_{\tau 0}}\frac{\partial^2 u_i}{\partial x_j \partial x_j}+\frac{(1-\beta)}{\mathrm{Re}_{\tau 0}}\frac{\partial \tau_{ij}}{\partial x_j}+\Delta p\,\delta_{i1}$$

構成方程式
Johnson-Segalmanモデル
$$\frac{\partial \tau_{ij}}{\partial t}+u_k\frac{\partial \tau_{ij}}{\partial x_k}=(1-\alpha)\left(\tau_{ik}\frac{\partial u_j}{\partial x_k}+\frac{\partial u_i}{\partial x_k}\tau_{kj}\right)-\alpha\left(\tau_{ik}\frac{\partial u_k}{\partial x_j}+\frac{\partial u_k}{\partial x_i}\tau_{kj}\right)$$
$$-\frac{\mathrm{Re}_{\tau 0}}{\mathrm{We}_{\tau 0}}f(\tau)\tau_{ij}+\frac{\mathrm{Re}_{\tau 0}}{\mathrm{We}_{\tau 0}}\left(\frac{\partial u_i}{\partial x_j}+\frac{\partial u_j}{\partial x_i}\right)$$

$f(\tau)=\frac{L^2}{L^2-3}+\frac{\mathrm{We}_{\tau 0}}{\mathrm{Re}_{\tau 0}}\frac{1}{L^2}\left|(1-2\alpha)\tau_{kk}\right|$: dumbbellの無限伸長を抑制するために導入したdumping項（Peterlin function）
→ FENE-Pモデル（α=0）

$f(\tau)=1$ → Oldroyd-Bモデル（α=0）

$$\mathrm{We}_{\tau 0}=\frac{\lambda u_\tau^2}{\nu_0}$$

Dependence of drag reduction rate on slip parameter

Drag reduction rate based on the flow : %DR

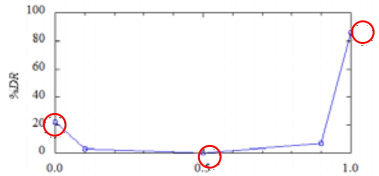

Run	α	%DR
V-1	0.0	22
V-2	0.1	3
V-3	0.5	0
V-4	0.9	7
V-6	1.0	86

Non-affinity α

Drag reduction

Non monotonous

Mean velocity profiles in pipe flow

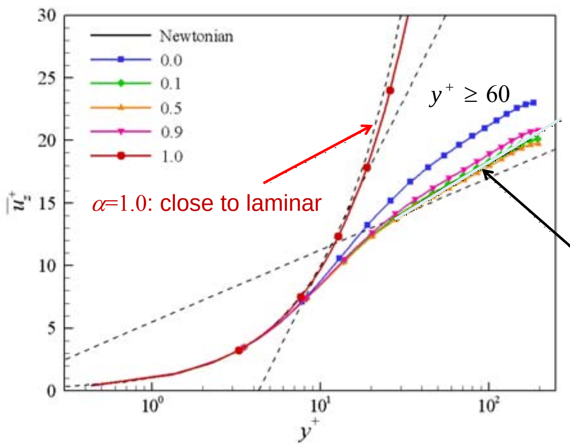

Larger drag reduction: Shifted upward

$\alpha = 0.5$: close to Newtonian

Mean shear stress profiles in pipe flow

Budget of the shear stress

$$\frac{r}{2}\frac{\partial \overline{p}}{\partial z}=\underbrace{-\overline{u_z' u_r'}}_{\text{Reynolds}}+\underbrace{\frac{\beta}{\mathrm{Re}_{\tau 0}}\frac{\partial \overline{u}_z}{\partial r}}_{\text{Viscous}}+\underbrace{\frac{1-\beta}{\mathrm{Re}_{\tau 0}}\overline{\tau}_{zr}}_{\text{Polymer stress}}$$

Newtonian　　α=0.0　　α=1.0

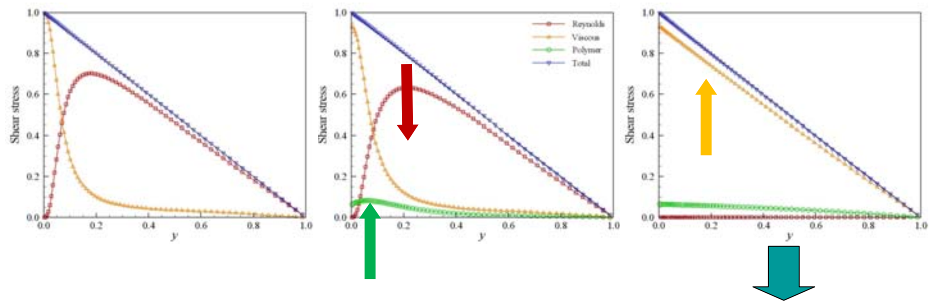

Relaminarization

非アフィン粘弾性流体における渦構造

Vortical Structures

ニュートン性流体

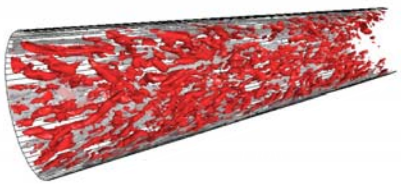

>多数の細かい渦構造

α=0.0

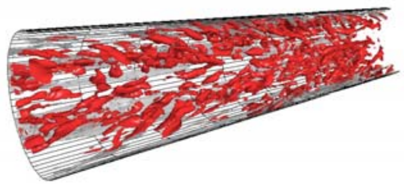

>細かい縦渦構造の減少

α=0.5

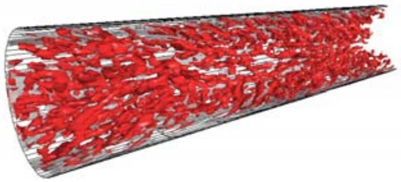

>ニュートン性流体の渦構造と類似

α=1.0（過渡期）

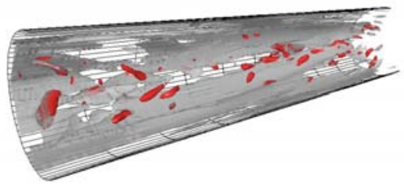

過渡後期 >渦構造の消失
>層流化

（赤：渦管，白：渦層）

抵抗削減機構 (α=0.0): Bulge out effect

Drag Reduction Mechanism at α=0.0: Bulge out effect

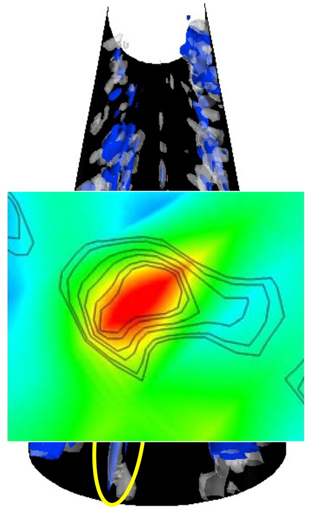

圧力に対する高分子寄与

$$\frac{\partial^2 p'_\tau}{\partial x_i^2} = \frac{1-\beta}{\mathrm{Re}_{\tau 0}} \frac{\partial^2 \tau'_{ij}}{\partial x_i \partial x_j}$$

p_τ：高分子圧力

(等値面)
白：渦管
青：高分子圧力

(等高線)
黒：渦管
青→赤：高分子圧力

高分子圧力が
渦管中央部で極大

圧力低下を抑制するbulge out効果

⇒ 渦管の伸長が抑制

Roles of normal stress difference on the vortex tube generation in pipe

$$\left(\tau_{rr} - \tau_{\theta\theta}\right) \approx \left(\tau_{++} - \tau_{--}\right)$$

Pressure gradient in the radial direction

$$r\frac{d}{dr}\left(p - \tau_{zz}\right) = r\frac{d}{dr}\left(\tau_{rr} - \tau_{zz}\right) + \underline{\left(\tau_{rr} - \tau_{\theta\theta}\right)} + \cdots$$

Weissenburg effect

$\left(\tau_{++} - \tau_{--}\right)$: predominantly negative

$$\therefore \frac{dp}{dr} < 0$$

Pressure bulges out in tube core region
⇒ Reduction of lowering of pressure in the tube core.
⇒ Reduction of growth of the tube.

Inhibition of the vortex generation

Distribution of $\left(\tau_{++} - \tau_{--}\right)$ on the tube

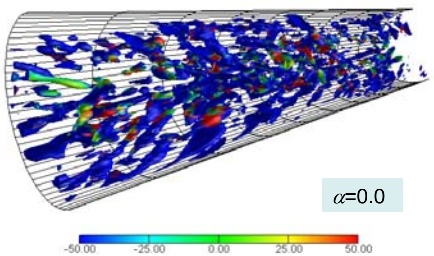

Streaky structure in pipe flow

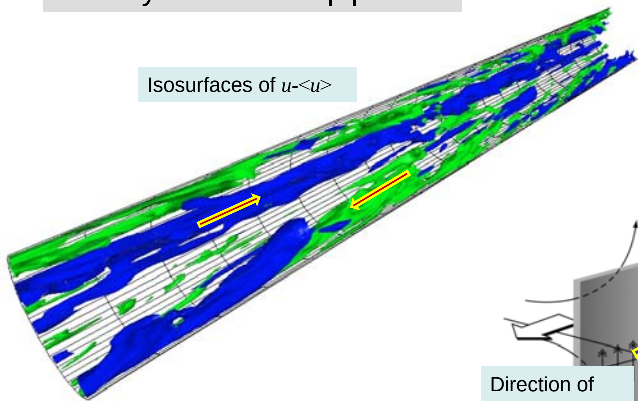

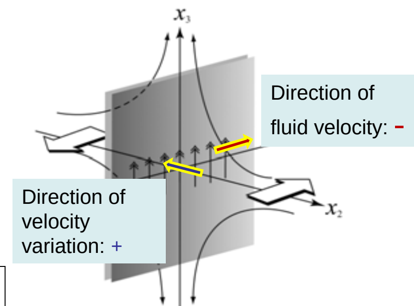

⇒ First normal stress difference
$$\left(\tau_{11} - \tau_{22}\right) \approx \left(\tau_{--} - \tau_{++}\right)$$

⇒ Second normal stress difference
$$\left(\tau_{22} - \tau_{33}\right) \approx \left(\tau_{++} - \tau_{ss}\right)$$

First and second normal stress differences along the vortex sheet

Similar to homogeneous isotropic turbulence

First: $(\tau_{11} - \tau_{22}) \approx (\tau_{--} - \tau_{++})$

Second: $(\tau_{22} - \tau_{33}) \approx (\tau_{++} - \tau_{ss})$

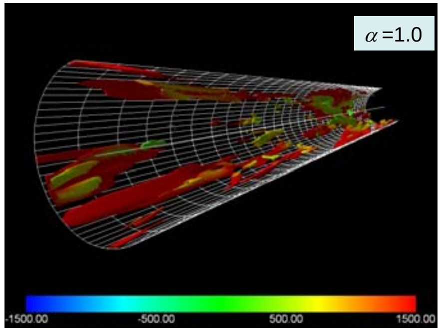

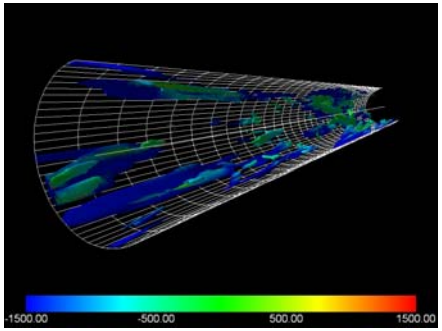

Predominantly positive

Predominantly negative

Stretching and alignment of the polymer molecules along the streamlines ⇒

⇒ Extra tension exerted along the sheet ⇒ Snap back of the sheet to the original form

Approximate solution of the JS model

Approximate solution with τ_{ij}= 0 at t =0 (Bird *et al*. 1987)

$$\tau_{ij}(t) \approx -\frac{\nu(1-\beta)}{\lambda}\int_0^t e^{-\frac{t-s}{\lambda}} 2S_{ij}(s)ds$$
$$+2\frac{\nu(1-\beta)}{\lambda}(1-\alpha)\int_0^t dr \int_0^r ds \;\; e^{-\frac{t-s}{\lambda}} 2\left(S_{ik}(s)\frac{\partial u_j}{\partial x_k}(r) + \frac{\partial u_i}{\partial x_k}(r) S_{kj}(s)\right)$$
$$-2\frac{\nu(1-\beta)}{\lambda}\alpha\int_0^t dr \int_0^r ds \;\; e^{-\frac{t-s}{\lambda}} 2\left(S_{ik}(s)\frac{\partial u_k}{\partial x_j}(r) + \frac{\partial u_k}{\partial x_i}(r) S_{kj}(s)\right)$$

Assume the steady state (the solution up to 3rd-order)

$$\tau_{ij} \approx -2\nu(1-\beta)S_{ij} + \lambda\nu(1-\beta)\{-(1-2\alpha)4S_{ik}S_{kj} + 2(S_{ik}\Omega_{kj} + S_{jk}\Omega_{ki})\}$$
$$+\lambda^2\nu(1-\beta)[-(1-2\alpha)^2 8S_{ik}S_{kl}S_{lj} + (1-2\alpha)\{(S_{ik}S_{kl}\Omega_{lj} + S_{jk}S_{kl}\Omega_{li}) - (\Omega_{ik}S_{kl}S_{lj} + \Omega_{jk}S_{kl}\Omega_{li})\}]$$
$$-2\lambda^2\nu(1-\beta)\{(S_{ik}\Omega_{kl}\Omega_{lj} + S_{jk}\Omega_{kl}\Omega_{li}) - (\Omega_{ik}S_{kl}\Omega_{lj} + \Omega_{jk}S_{kl}\Omega_{li})\}$$

Analogous to the nonlinear model for the Reynolds stress tensor

Approximate solution of the JS model

Approximate solution with τ_{ij}= 0 at t =0 (Bird *et al*. 1987)

$$\tau_{ij}(t) \approx -\frac{\nu(1-\beta)}{\lambda}\int_0^t e^{-\frac{t-s}{\lambda}} 2S_{ij}(s)ds$$
$$+2\frac{\nu(1-\beta)}{\lambda}(1-\alpha)\int_0^t dr \int_0^r ds \;\; e^{-\frac{t-s}{\lambda}} 2\left(S_{ik}(s)\frac{\partial u_j}{\partial x_k}(r) + \frac{\partial u_i}{\partial x_k}(r) S_{kj}(s)\right)$$
$$-2\frac{\nu(1-\beta)}{\lambda}\alpha\int_0^t dr \int_0^r ds \;\; e^{-\frac{t-s}{\lambda}} 2\left(S_{ik}(s)\frac{\partial u_k}{\partial x_j}(r) + \frac{\partial u_k}{\partial x_i}(r) S_{kj}(s)\right)$$

Assume the steady state (the solution up to 2nd-order)

$$\tau_{ij} \approx -\nu(1-\beta)2S_{ij}$$
$$+2\lambda\nu(1-\beta)\{-(1-2\alpha)2S_{ik}S_{kj} + (S_{ik}\Omega_{kj} + S_{jk}\Omega_{ki})\}$$

Analogous to the nonlinear model for the Reynolds stress tensor

Approximate solution of the JS model (up to 3rd-order)

Production term of the solvent kinetic energy

$$P_k = \tau_{ij}S_{ij} \approx -2\nu(1-\beta)S_{ij}S_{ji}$$
$$+\lambda\nu(1-\beta)\{-(1-2\alpha)4S_{ik}S_{kj}S_{ji}\}$$ Derivative skewess
$$+\lambda^2\nu(1-\beta)[-(1-2\alpha)^2 8S_{ik}S_{kl}S_{lj}S_{ji}]$$ Derivative flatness < 0
$$-2\lambda^2\nu(1-\beta)A_{ij}A_{ji}$$ Large in sheet region < 0

Non-monotonical dependence on α

Production term of the elastic energy

$$P_e = \pm(1-2\alpha)(-P_k) \quad \begin{cases} + : \alpha \le 0.5 \\ - : \alpha > 0.5 \end{cases} \quad \left(k_p = \pm\frac{1}{2}\tau_{ii}\right)$$

Approximate solution of the JS model (up to 2nd-order)

Production term of the solvent kinetic energy

$$\tau_{ij}S_{ij} \approx -\nu(1-\beta)2S_{ij} - 4\lambda\nu(1-\beta)(1-2\alpha)S_{ik}S_{kj}S_{ij}$$

α =0.0

$$\tau_{ij}S_{ij} \approx -\nu(1-\beta)2S_{ij}S_{ij} - 4\lambda\nu(1-\beta)\underline{S_{ik}S_{kj}S_{ij}}$$

< 0

Effective shear viscosity

Shear thinning

α =1.0

$$\tau_{ij}S_{ij} \approx -\nu(1-\beta)2S_{ij}S_{ij} + 4\lambda\nu(1-\beta)\underline{S_{ik}S_{kj}S_{ij}}$$

< 0

Effective shear viscosity

Comparison of energy production terms (Full JS model)

	α=0 (Oldroyd-B)	α=0.5	α=1 (Oldroyd-A)
Solvent kinetic energy $u_iu_i/2$	$P_s=\tau_{ij}S_{ji}<0$ $u_iu_i/2$ ↘	$P_s=\tau_{ij}S_{ji}$ small	$P_s=\tau_{ij}S_{ji}<0$ $u_iu_i/2$ ↘
Elastic energy k_p	$P_e=-\tau_{ij}S_{ji}>0$ $-\tau_{ii}/2$ ↗	$P_e=-(1-2\alpha)\,\tau_{ik}S_{ik}=0$	$P_e=-\tau_{ij}S_{ji}<0$ $-\tau_{ii}/2$ ↗
$k_p = \pm\frac{1}{2}\tau_{ii}\begin{cases}+:\alpha\le 0.5\\ -:\alpha>0.5\end{cases}$	Reduction of kinetic Energy and conversion to elastic energy	Close to Newtonian: Solid-body rotation with no stretching	Reduction of kinetic Energy and conversion to elastic energy

Limitations of 2nd-order approximate JS model

2nd-order steady solution of the JS model

$$\tau_{ij} \approx 2\lambda\nu(1-\beta)\{-(1-2\alpha)2S_{ik}S_{kj} + (S_{ik}\Omega_{kj} + S_{jk}\Omega_{ki})\}$$

3rd-order steady solution (Bird *et al.* 1987)

$$\tau_{ij} \approx 2\lambda\{-(1-2\alpha)2S_{ik}S_{kj} + (S_{ik}\Omega_{kj} + S_{jk}\Omega_{ki})\}$$
$$-2\lambda^2\{4S_{ik}S_{kl}S_{lj} + (S_{ik}\Omega_{kl}\Omega_{lj} + S_{jk}\Omega_{kl}\Omega_{li}) - (\Omega_{ik}S_{kl}\Omega_{lj} + \Omega_{jk}S_{kl}\Omega_{li})\}$$
$$-2\lambda^2(2\alpha-1)\{(S_{ik}\Omega_{kl}S_{lj} + S_{jk}\Omega_{kl}S_{li}) + 3(S_{ik}S_{kl}\Omega_{lj} + S_{jk}S_{kl}\Omega_{li})\}$$

Elastic energy production term (3rd-order)

$$P_s \approx -(1-2\alpha)^2\nu(1-\beta)4\lambda S_{ik}S_{kj}S_{ji}$$
$$+(1-2\alpha)\nu(1-\beta)2\lambda^2\{\underline{4S_{ik}S_{kl}S_{lj}S_{ji}} + 2S_{ik}\Omega_{kl}\Omega_{lj}S_{ji} - 2\Omega_{ik}S_{kl}\Omega_{lj}S_{ji}\}$$

$P_e<0$, 2nd-order

$$\tau_{ij} \approx 2\lambda\{-(1-2\alpha)2S_{ik}S_{kj}S_{ji}\}$$
$$-2\lambda^2\{4S_{ik}S_{kl}S_{lj}S_{ji} + (S_{ik}\Omega_{kl}\Omega_{lj} + S_{jk}\Omega_{kl}\Omega_{li}) - (\Omega_{ik}S_{kl}\Omega_{lj} + \Omega_{jk}S_{kl}\Omega_{li})\}$$

3rd-order: $P_e>0$ for $0<\alpha<0.5$, $P_e<0$ for $0.5<\alpha<1$

3次定常近似解によるエネルギー変換の見積もり

Energy Exchange (3rd-order Steady Solution)

$$P_k^{(\tau)} = -\frac{1-\beta}{\mathrm{Re}_{\tau 0}}\tau_{ij}^{(3)}S_{ij} = -\frac{1-\beta}{\mathrm{Re}_{\tau 0}}2S_{ij}S_{ij} - \frac{(1-\beta)\mathrm{We}_{\tau 0}}{\mathrm{Re}_{\tau 0}^2}4(1-2\alpha)S_{ik}S_{kj}S_{ji}$$
$$\boxed{-\frac{(1-\beta)\mathrm{We}_{\tau 0}^2}{\mathrm{Re}_{\tau 0}^3}8(1-2\alpha)^2 S_{ik}S_{kl}S_{lj}S_{ji}}\boxed{-\frac{(1-\beta)\mathrm{We}_{\tau 0}^2}{\mathrm{Re}_{\tau 0}^3}2A_{ij}A_{ji}}$$

> 第3項

$S_{ik}S_{kl}S_{lj}S_{ji}$: derivative skewness

と比較して大きな正値

> αに対する非単調依存，DNSと整合

> 第4項

渦層： $[A_{ij}]_+ \approx \sqrt{A_{ij}A_{ji}/2}$

(Horiuti *et al.*, 2005)

> 渦層上で$P_k^{(\tau)}$ の負値の増加，DNSと整合

弾性エネルギー生成項

上符号： $\alpha < 0.5$
下符号： $\alpha > 0.5$

$$P_e^{(t)} = \pm(1-2\alpha)(-P_k^{(\tau)})$$

：渦層上での生成

Comparison of energy production terms (2nd-order model)

	α=0 (Oldroyd-B)	α=0.5	α=1 (Oldroyd-A)
Solvent kinetic energy $u_iu_i/2$	$P_s = \tau_{ik}S_{ik} > 0$	$P_s = \tau_{ik}S_{ik} = 0$	$P_s = \tau_{ik}S_{ik} < 0$ $u_iu_i/2$ $\searrow$
Elastic energy $-\tau_{ii}/2$	$P_e = -\tau_{ik}S_{ik} < 0$	$P_e = -(1-2\alpha)\ \tau_{ik}S_{ik}$ $= 0$	$P_e = \tau_{ik}S_{ik} < 0$ $-\tau_{ii}/2$ $\searrow$
	Enhancement of turbulence	Close to Newtonian	Reduction of turbulence

Summary

- A stretched spiral vortex is identification using DNS data for homogeneous isotropic turbulence. Its genesis, growth and annihilation are elucidated .
- Existence of two symmetric modes and a third asymmetric of configurations is extracted. They are achieved through the interaction of several sheets.
- Mechanism of mode transition and persistence of each mode is shown.
- By tightening of the spiral turns, spiral sheets are stretched to extreme lengths. Intense energy cascade and dissipation occurs along the spiral sheets.
- Effect of viscoelasticity on the formation of spiral vortex is studied using the constitutive equation for the polymer stress. It is shown that viscoelastisity works to resist extensional motions of the turbulent flow.

Interaction of multiple tubular vortical structures

(Transverse: Holm & Kerr 2002; Anti parallel: Goto 2008)

Reconnection of two orthogonally offset cylindrical vortices

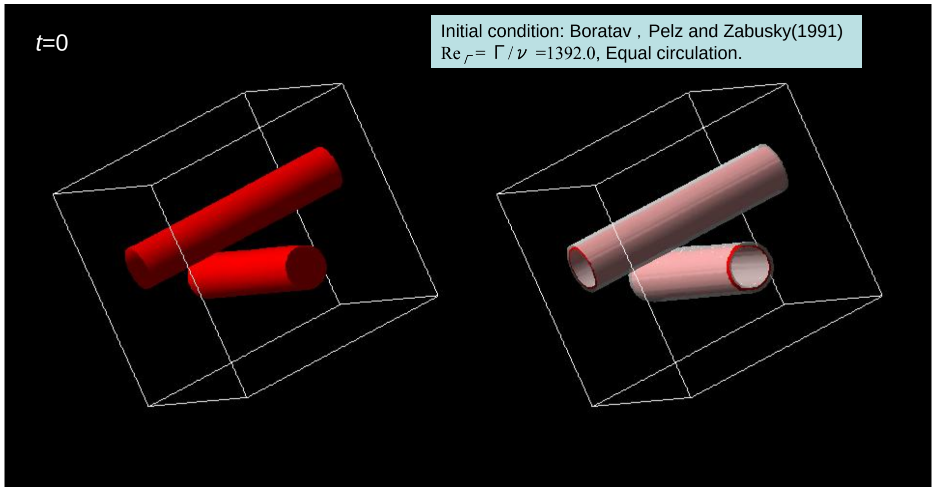

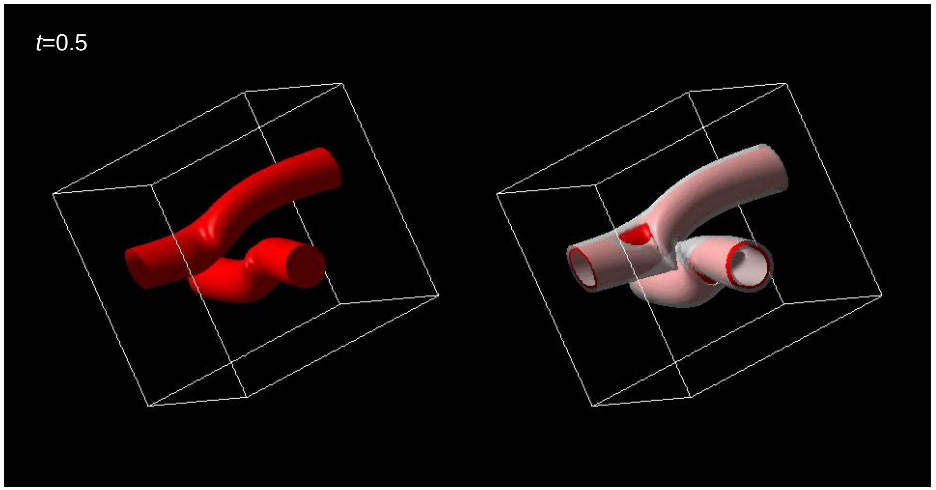

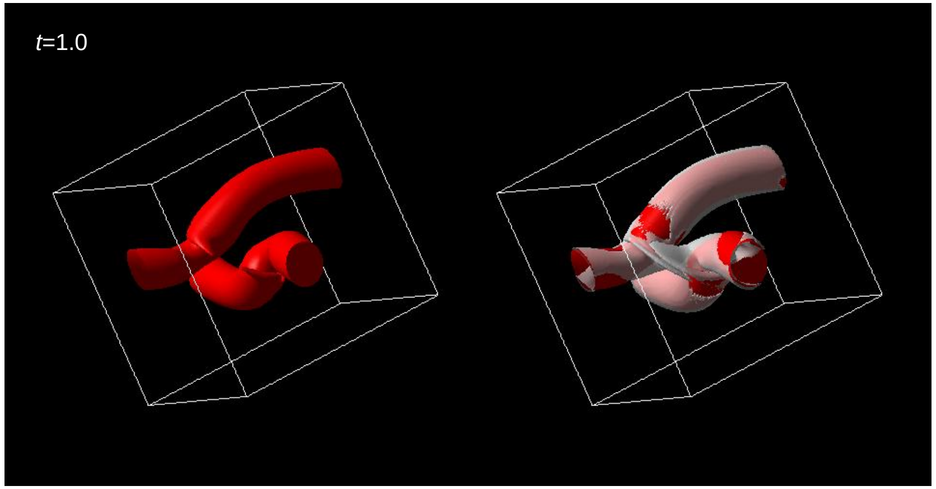
t=1.0

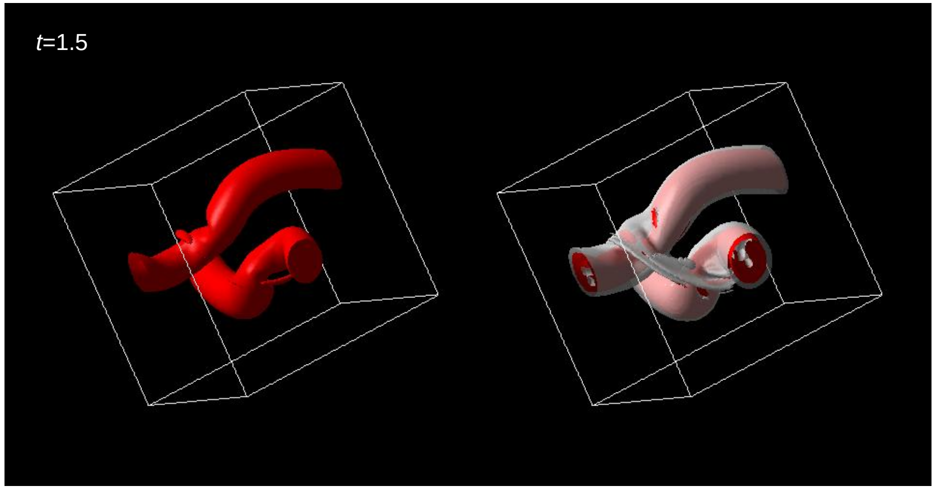
t=1.5

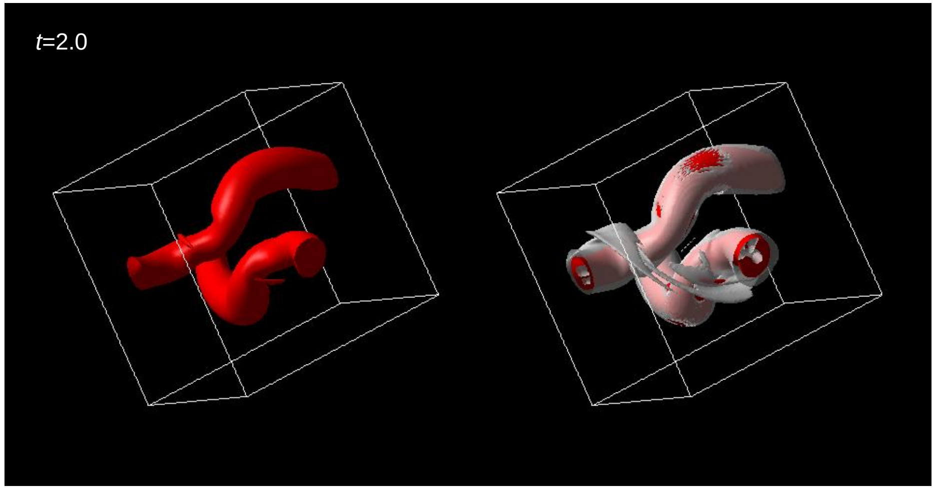
t=2.0

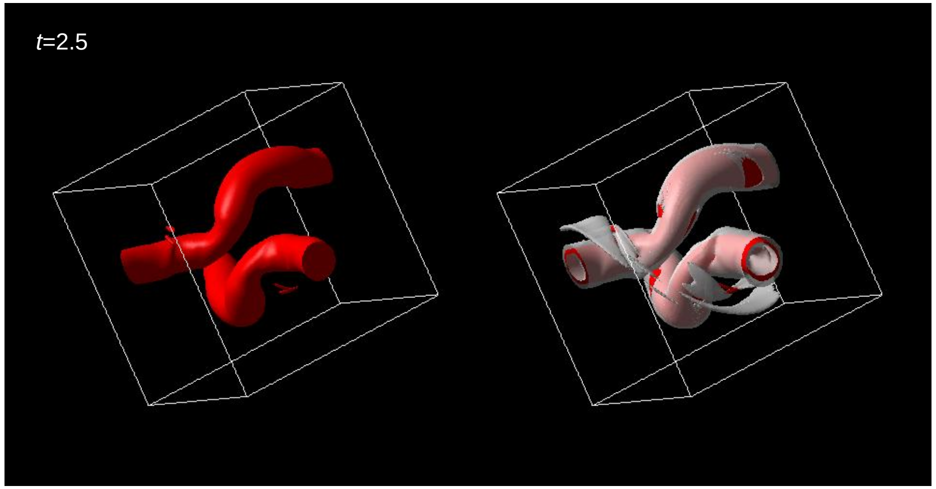
t=2.5

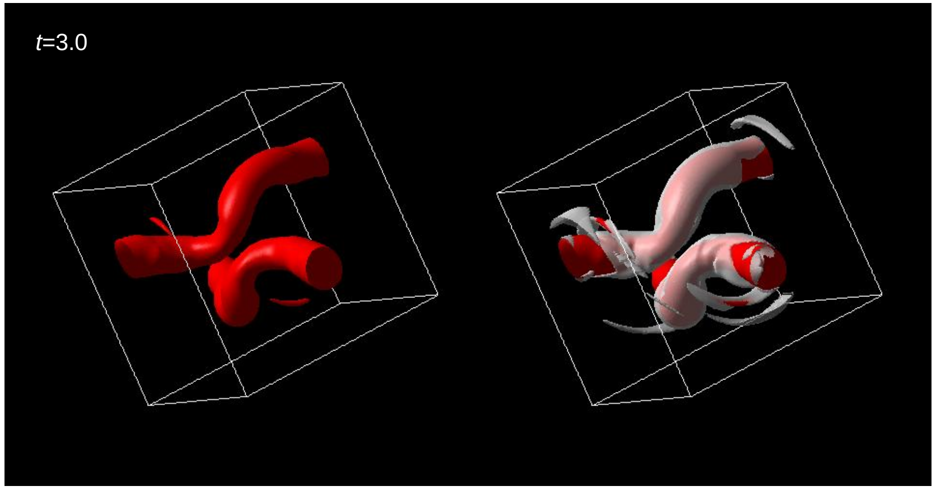
t=3.0

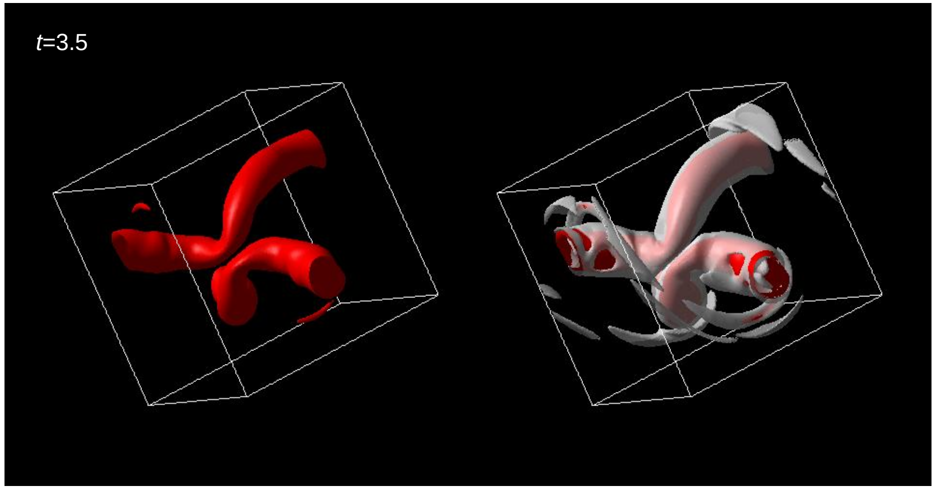
t=3.5

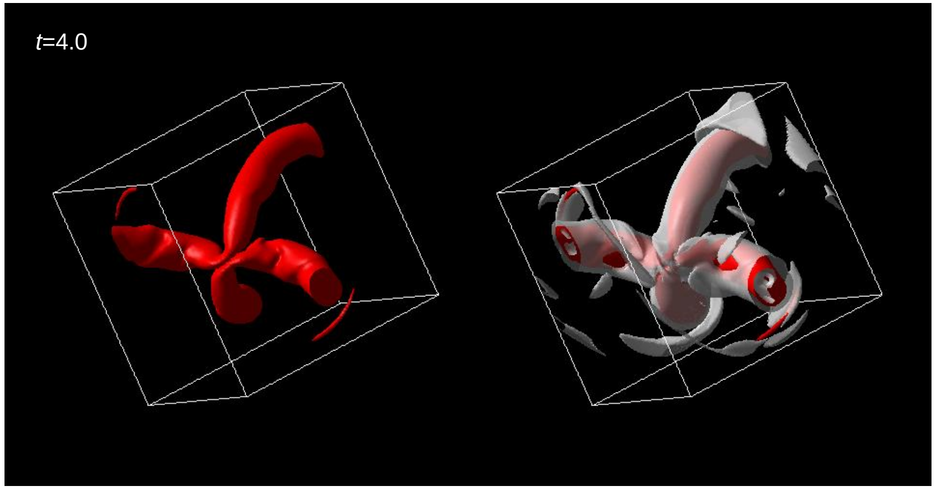
t=4.0

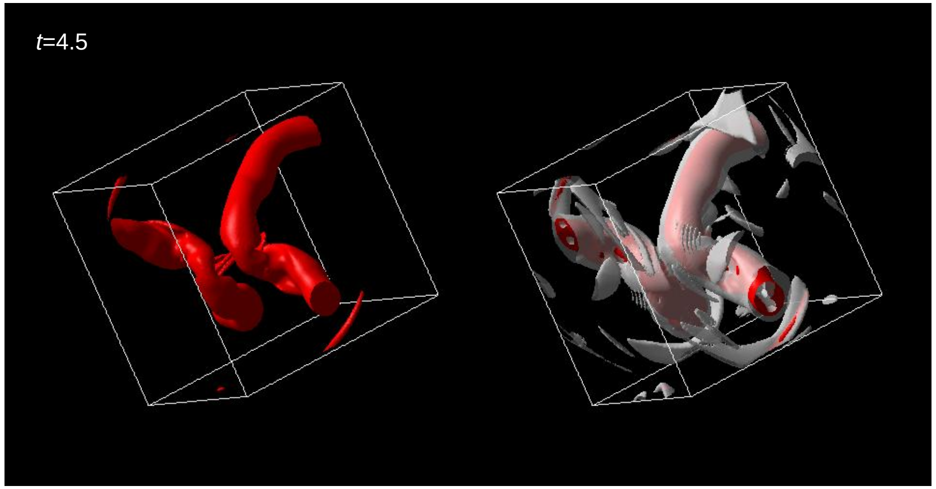
t=4.5

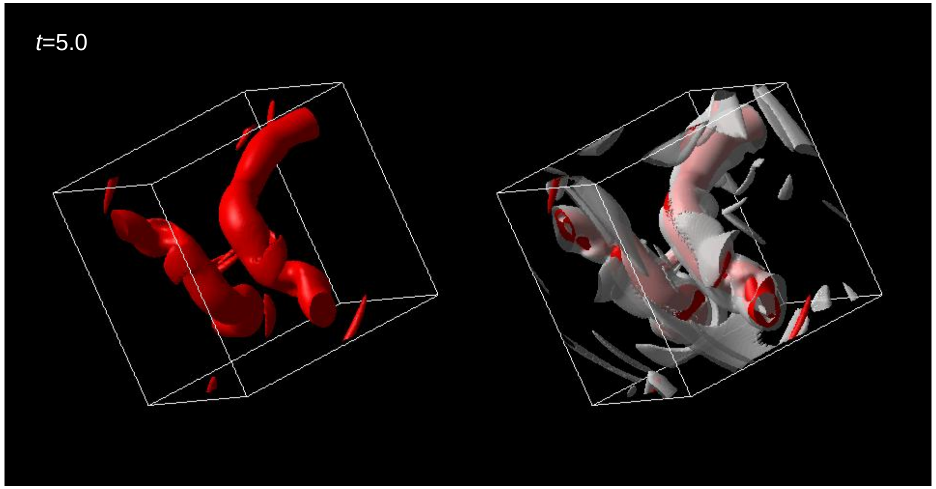
t=5.0

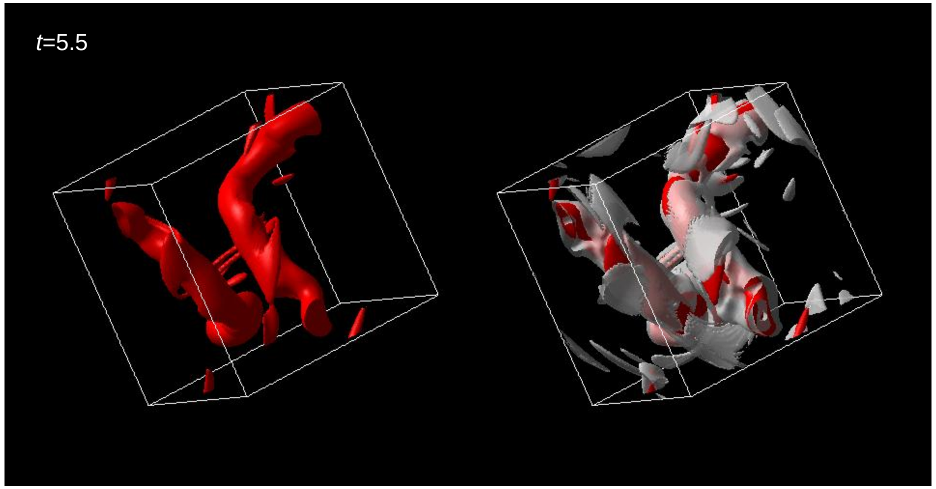
t=5.5

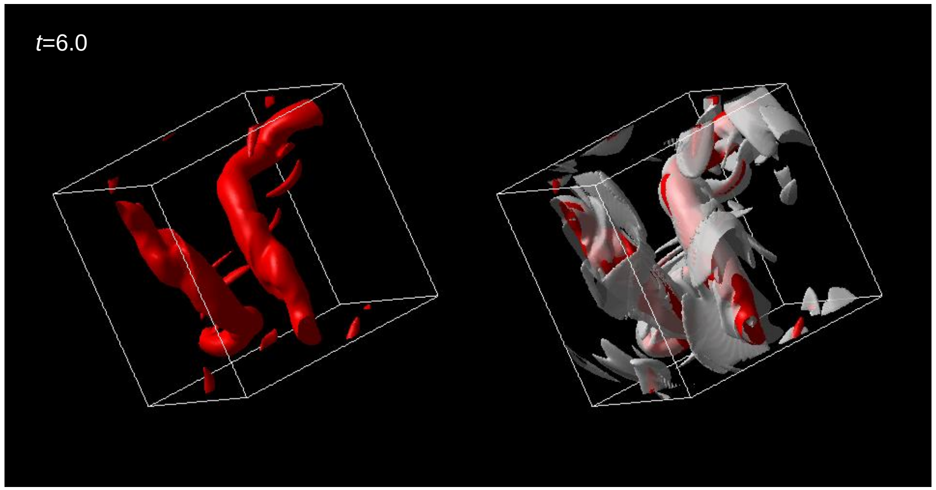
t=6.0

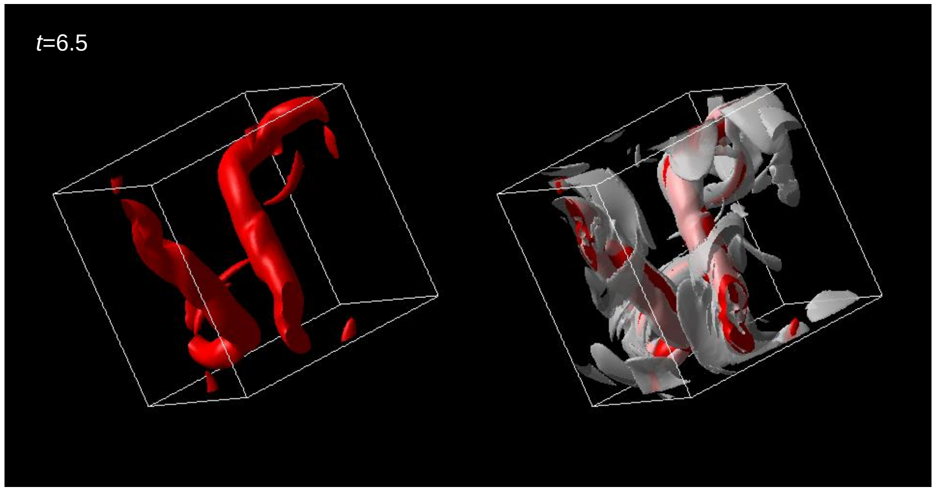
t=6.5

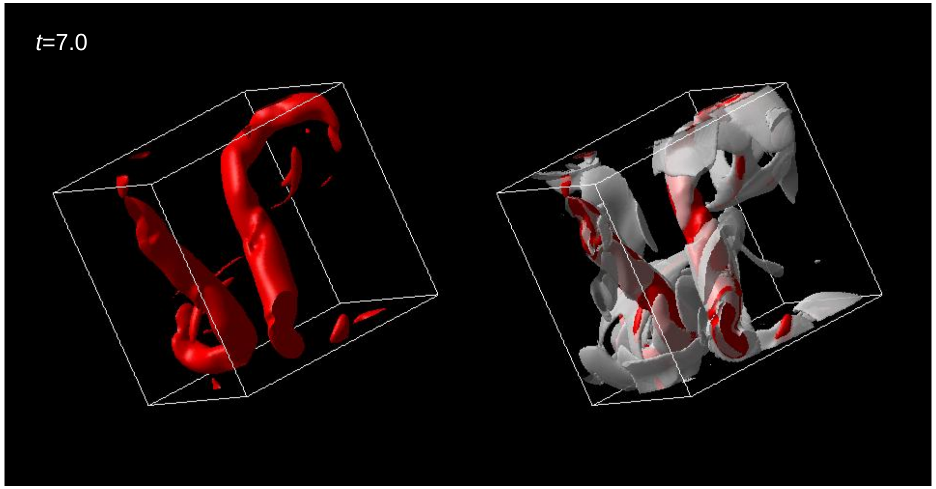

Transition of topology during the reconnection process

Time evolution of helicity density and P_h^s term

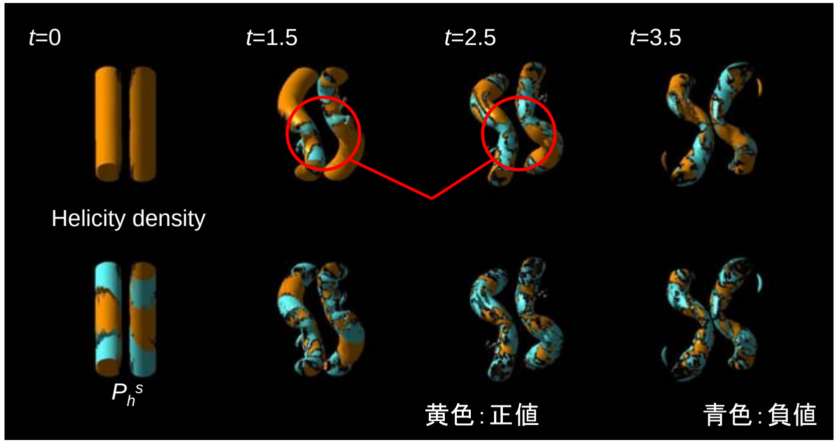

Intense dissipation event via an interaction and reconnection of the two vortices

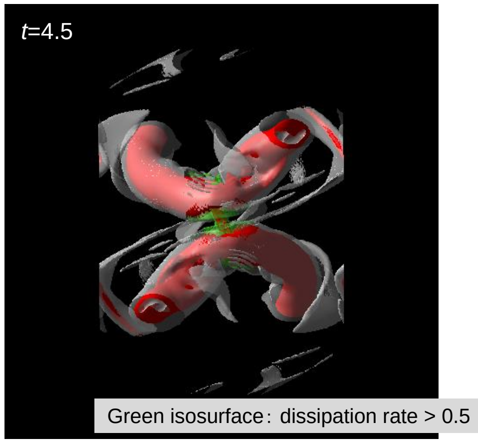

Intense dissipation is generated along the stretched sheets in the vicinity of the reconnection point.

Candidate for non-affine polymers

1. DNA: exhibits marked drag reduction

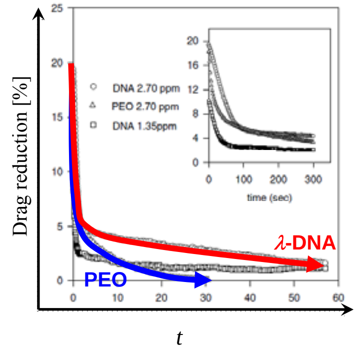

2. Surfactant (with high concentration)

Conclusion

- A stretched spiral vortex is identification using DNS data for homogeneous isotropic turbulence. Its genesis, growth and annihilation are elucidated .
- Aside from the two symmetric modes of configurations studied in previous works, a third asymmetric mode is extracted, which is achieved through the interaction of several sheets.
- By tightening of the spiral turns, spiral sheets are stretched to extreme lengths. Intense dissipation occurs along the spiral sheets. The local dissipation rate exhibits a strong intermittency.
- At a higher Reynolds number, the hierarchical cluster of spiral vortices is formed due to the instability cascade induced by the stretching of vortex sheets.
- Similarity in the fractal properties of the vortex sheet region and the dissipative region is shown.

Analogy with turbulence models (LES/RANS)

Difference in the sign of the $-(S_{ik}\Omega_{kj}+S_{jk}\Omega_{ki})$ term (Horiuti 2003)

Nonlinear model (Newtonian case)

$$\tau_{ij} \approx \frac{\bar{\Delta}^2}{12}\left\{\left(\bar{S}_{ik}\bar{S}_{kj} - \bar{\Omega}_{ik}\bar{\Omega}_{kj}\right) - \left(\bar{S}_{ik}\bar{\Omega}_{kj} + \bar{S}_{jk}\bar{\Omega}_{ki}\right)\right\}$$

2nd-order steady solution of the JS model (Viscoelastic case)

$$\tau_{ij} \approx 2\lambda\nu(1-\beta)\left\{-(1-2\alpha)2S_{ik}S_{kj} + \boxed{\left(S_{ik}\Omega_{kj} + S_{jk}\Omega_{ki}\right)}\right\}$$

Assessment of 2nd-order model in homogeneous isotropic turbulence

256^3 grid points, β= 0.8, λ= 0.36, We= 7.8, Re_λ=80

Classification of structures in turbulent flows

Tube-like structure similar to Burgers' vortex tube

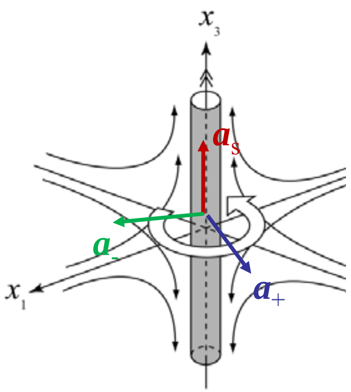

Sheet-like structure similar to Burgers' vortex layer

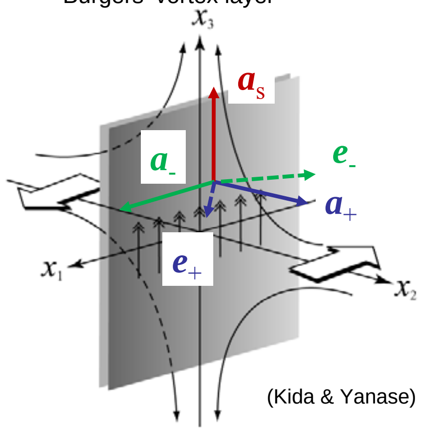

(Kida & Yanase)

Comparison of energy production terms (2nd-order model)

	α=0 (Oldroyd-B)	α=0.5	α=1 (Oldroyd-A)
Solvent kinetic energy $u_iu_i/2$	$P_s = \tau_{ik}S_{ik}$ $-4(1-\beta)\nu\lambda S_{ik}S_{kj}S_{ji} > 0$	$P_s = \tau_{ik}S_{ik} = 0$	$P_s = \tau_{ik}S_{ik}$ $=4(1-\beta)\nu\lambda S_{ik}S_{kj}S_{ji} < 0$ $u_iu_i/2$
Elastic energy $-\tau_{ii}/2$	$P_e = -\tau_{ik}S_{ik}$ $4(1-\beta)\nu\lambda S_{ik}S_{kj}S_{ji} < 0$	$P_e = -(1-2\alpha)\,\tau_{ik}S_{ik}$ $= 0$	$P_e = \tau_{ik}S_{ik}$ $=4(1-\beta)\nu\lambda S_{ik}S_{kj}S_{ji} < 0$ $-\tau_{ii}/2$
	Enhancement of turbulence	Close to Newtonian	Reduction of turbulence

Eigenvaluevalues for A_{ij}

- Characteristic equation

$$x^3 - \frac{1}{2}\left(A_{ij}A_{ji}\right)x - \frac{1}{3}\left(A_{ij}A_{jk}A_{ki}\right) = 0 \qquad \mathrm{tr}[A_{ij}] = 0$$

where

$$A_{ij}A_{ji} = \underline{-6S_{ik}\Omega_{kl}\Omega_{lj}S_{ji} + S_{ik}S_{ki}\Omega_{jl}\Omega_{lj}}$$

$$= \frac{\omega_z^2}{2}(\sigma_+ - \sigma_-)^2 + \frac{\omega_+^2}{2}(\sigma_z - \sigma_-)^2 + \frac{\omega_-^2}{2}(\sigma_z - \sigma_+)^2,$$

$$A_{ij}A_{jk}A_{ki} = \frac{3}{4}(\sigma_+ - \sigma_-)(\sigma_z - \sigma_-)(\sigma_z - \sigma_+)\omega_z\omega_+\omega_-.$$

- DNS data shows that $A_{ij}A_{ji} \gg A_{ij}A_{jk}A_{ki}$, thus

$$[A_{ij}]_\pm \cong \pm\sqrt{A_{ji}A_{ji}/2}, \quad [A_{ij}]_z \cong 0$$

Invariants of fourth-order moments of velocity gradients

- $I_1 = (S_{ik}S_{ki})(S_{jl}S_{lj})$

  $I_2 = -2S_{ik}S_{ki}\Omega_{jl}\Omega_{lj}$

  $I_3 = 4S_{ik}\Omega_{kj}\Omega_{jl}S_{li} - 2S_{ik}S_{ki}\Omega_{jl}\Omega_{lj}$

  $I_4 = 8\Omega_{ik}\Omega_{kl}\Omega_{lj}\Omega_{ji}$ (Siggia, 1981)

  All fourth-order moments are linear combination of $\boldsymbol{I}_i$ (i=1,2,3,4).

- $$A_{ij}A_{ji} = I_2 - \frac{3}{2}I_3$$

Fractal properties of the vortex sheet and dissipation region (1)

Box counting for individual dissipative structures

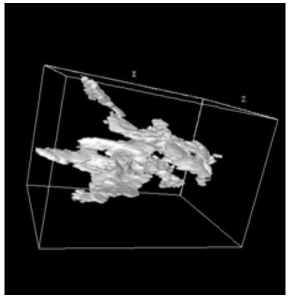

A set of adjucent points satisfying the thresholding criterion

Moisy and Jimenez (2004)

$N\varepsilon$: Number of boxes containing some point of large dissipative structures

$N\varepsilon(L) \sim L^{-d}$ $\quad$ d: Fractal dimension

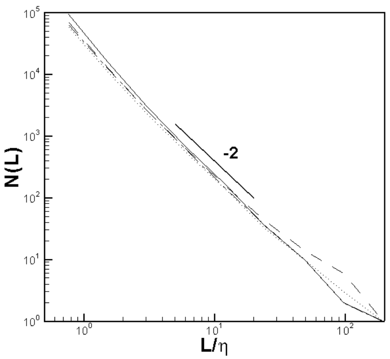

Fitting in the range, 6 $\overline{\eta}$ <L< L_{max}

Fractal properties of the vortex sheet and dissipation region (2)

Mean value of $d\varepsilon$ averaged over structures as a function of threshold and fractal dimension for $[A_{ij}]_+$

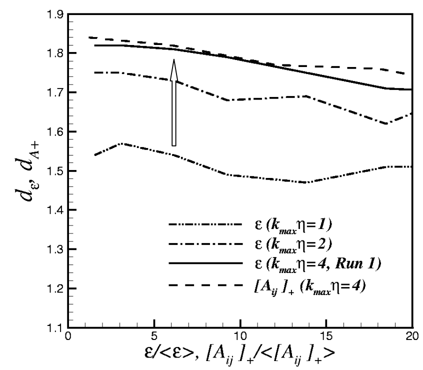

Correlation between the vortex sheet and dissipation rate

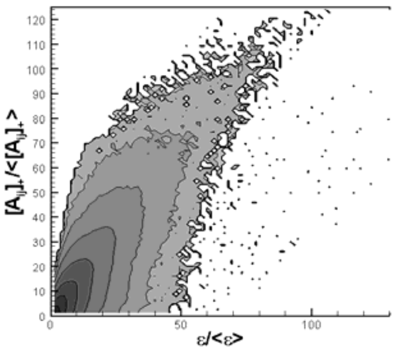

C.C~ 0.83

Statistical property of the educed region: Fractality

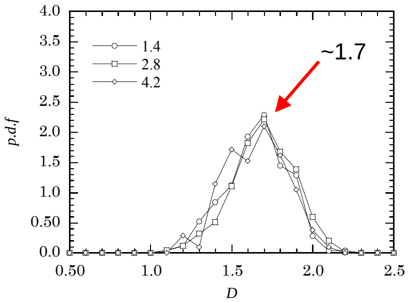

Strain rate S_{ii}

Sheet-like objects

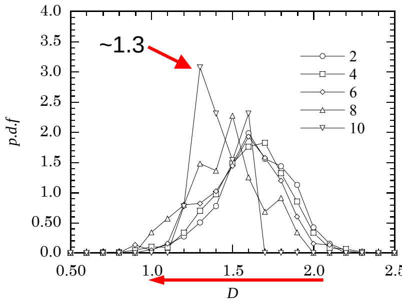

Vorticity Ω_{ij}

Filamentary objects

512^3 Forced case (Moisy and Jimenez 2004)

Statistical property of the educed region: Fractality of $[A_{ij}]_+$

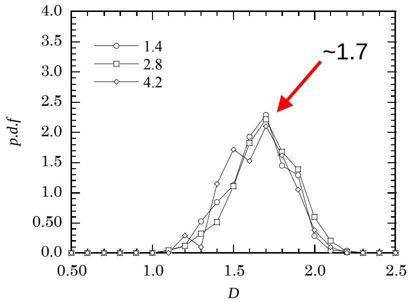

Strain rate S_{ii}

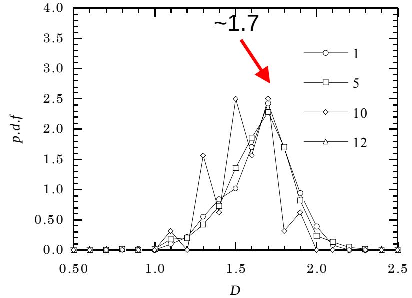

$[A_{ij}]_+$

Fractal dimension of $[A_{ij}]_+$ ~ 1.7, close to that of strain rate.

➡ $[A_{ij}]_+$ educes the region in which intense dissipation takes place.

W

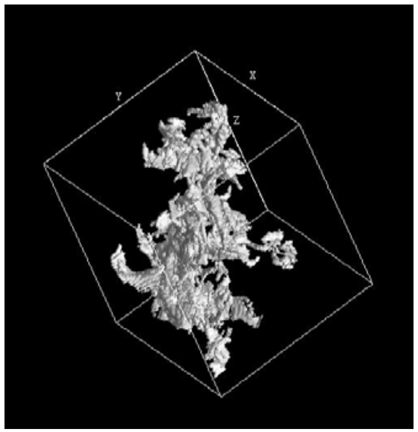

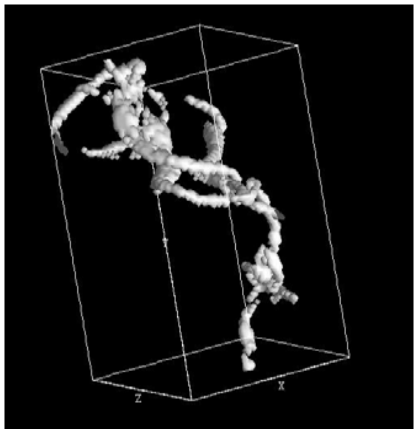

W(512^3, τ=3.0_2nd, D=1.96) W(512^3, τ=8.0_1nd, D=1.55)

S

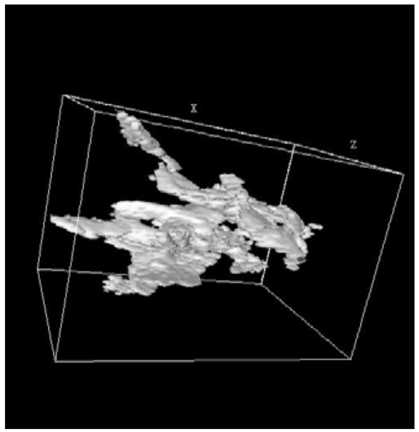

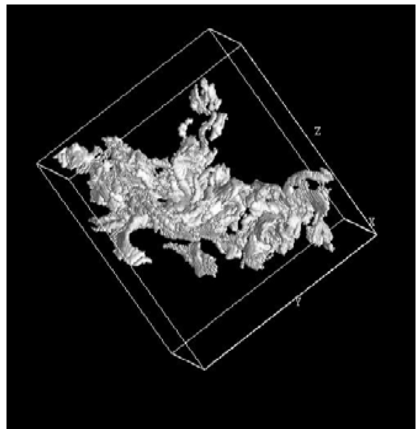

S(512^3, τ=2.8_2nd, D=1.89) S(5123, t=4.2_2nd, D=2.01)

SWSW

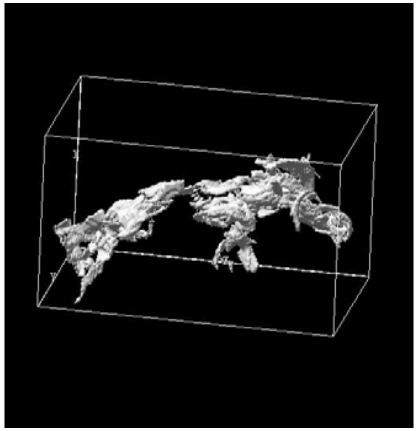

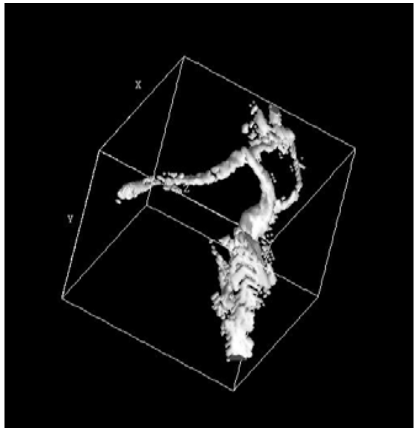

SWSW(512^3, τ=2.0_2nd, D=1.92)　SWSW(512^3, τ=10.0_2nd, D=1.68)

マルチフラクタル解析

- Subbox average

$$p_i = \left(\frac{\varepsilon^{(i)}}{\varepsilon_L}\right)\left(\frac{r}{L}\right)^d \qquad (\, d = 3\,)$$

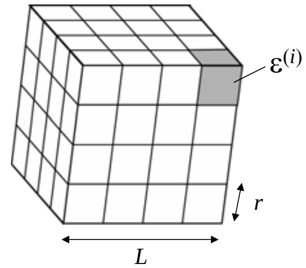

- 一般化次元

$$D_q = \lim_{r/L \to 0} \frac{\ln \sum_i p_i^q}{(q-1)\ln(r/L)}$$

D_qは$(\Sigma_i p_i^q)^{(1/(q-1))}$と r/L のスケーリング関係より求まる.

散逸率, $[A_{ij}]_+$, $\Omega_{ik}\Omega_{ik}$のスケーリング

Forcing, $N = 512^3$, $Re_\lambda \sim 244.5$

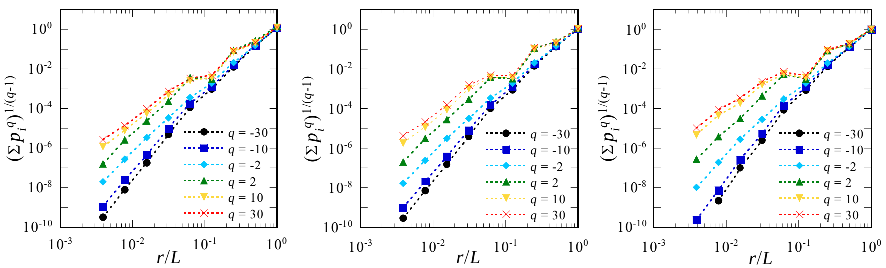

散逸率　$[A_{ij}]_+$　$\Omega_{ik}\Omega_{ik}$

慣性小領域を越えてスケーリングが成り立つ.

マルチフラクタル特性

- q-Dq曲線
  - 散逸構造と渦層構造は相似な分布

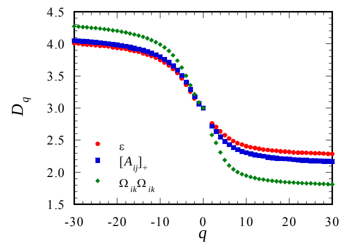

- 等α集合のフラクタル次元 $f(\alpha(q))$

$$p_i \sim \left(\frac{r}{L}\right)^{\alpha-1+d},$$

$$\alpha(q) = \frac{d}{dq}\{(q-1)(D_q - d + 1)\},$$

$$f(\alpha(q)) = q\alpha(q) - (q-1)D_q + q(d-1).$$

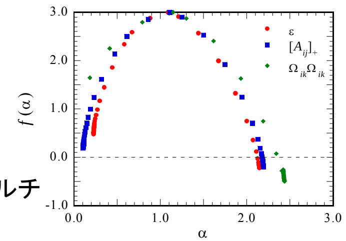

散逸構造と渦層構造は相似なマルチフラクタル特性を有している.

ひずみ速度と渦度のジョイント・マルチフラクタル

- 結合一般化次元 $D(q, p)$

$$\left(\frac{r}{L}\right)^{d(q+p)} \sum_i \left(\frac{s_r^{(i)}}{s_L}\right)^q \left(\frac{w_r^{(i)}}{w_L}\right)^p = \left(\frac{r}{L}\right)^{-(q-1)(p-1)D(q,p)}, \quad \frac{r}{L} \to 0$$

Subbox 内の平均ひずみ速度，平均渦度 : $s_r^{(i)}$, $w_r^{(i)}$

ひずみ速度，渦度の全空間平均 : s_L, w_L

- 等α，β集合のフラクタル次元 $f(\alpha, \beta)$

$$\tau(q, p) = -(q-1)(p-1)D(q, p)$$

$$\alpha(q, p) = \frac{\partial}{\partial q}\tau(q, p) + 1 - d,$$

$$\beta(q, p) = \frac{\partial}{\partial p}\tau(q, p) + 1 - d,$$

$$f(\alpha, \beta) = -\tau(q, p) + (\alpha - 1 + d)q + (\beta - 1 + d)p.$$

ひずみ速度と渦度の結合フラクタル次元

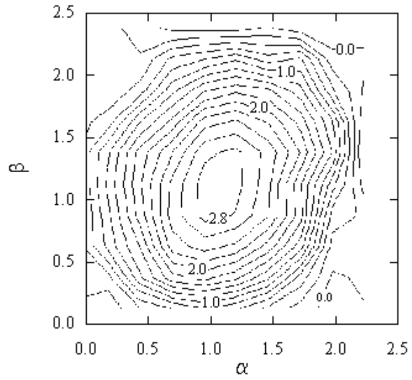

DNSの結果

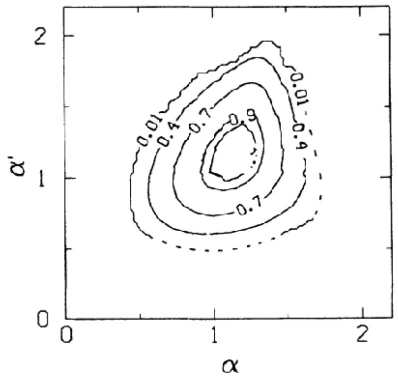

Menevau *et al*.(1990)の境界層実験の結果